Dixon WJ. 1980. Efficient analysis of experimental observations. Annu Rev Pharmacol Toxicol 20:441–462.
Hide I, Tanaka M, Inoue A, Nakajima K, Kohsaka S, Inoue K, Nakata Y. 2000. Extracellular ATP triggers tumor necrosis factor-alpha release from rat microglia. J Neurochem 75:965–972.
Honore P, Rogers SD, Schwei MJ, Salak-Johnson JL, Luger NM, Sabino MC, Clohisy DR, Mantyh PW. 2000. Murine models of inflammatory, neuropathic and cancer pain each generates a unique set of neurochemical changes in the spinal cord and sensory neurons. Neuroscience 98:585–598.
Ji RR, Samad TA, Jin SX, Schmoll R, Woolf CJ. 2002. p38 MAPK activation by NGF in primary sensory neurons after inflammation increases TRPV1 levels and maintains heat hyperalgesia. Neuron 36:57–68.
Kim SH, Chung JM. 1992. An experimental model for peripheral neuropathy produced by segmental spinal nerve ligation in the rat. Pain 50:355–363.
Kim SY, Bae JC, Kim JY, Lee HL, Lee KM, Kim DS, Cho HJ. 2002. Activation of p38 MAP kinase in the rat dorsal root ganglia and spinal cord following peripheral inflammation and nerve injury. NeuroReport 13:2483–2486.
Koistinaho M, Koistinaho J. 2002. Role of p38 and p44/42 mitogen-activated protein kinases in microglia. Glia 40:175–183.
Lee SH, Park J, Cho Y, Han PL, Lee JK. 2000. Constitutive activity and differential localization of p38alpha and p38beta MAPKs in adult mouse brain. J Neurosci Res 60:623–631.
Ma W, Quirion R. 2002. Partial sciatic nerve ligation induces increase in the phosphorylation of extracellular signal-regulated kinase (ERK) and c-Jun N-terminal kinase (JNK) in astrocytes in the lumbar spinal dorsal horn and the gracile nucleus. Pain 99:175–184.
Malmberg AB, Chen C, Tonegawa S, Basbaum AI. 1997. Preserved acute pain and reduced neuropathic pain in mice lacking PKCγ. Science 278:279–283.
Maruyama M, Sudo T, Kasuya Y, Shiga T, Hu B, Osada H. 2000. Immunolocalization of p38 MAP kinase in mouse brain. Brain Res 887:350–358.
Murashov AK, Ul Haq I, Hill C, Park E, Smith M, Wang X, Goldberg DJ, Wolgemuth DJ. 2001. Crosstalk between p38, Hsp25 and Akt in spinal motor neurons after sciatic nerve injury. Brain Res Mol Brain Res 93:199–208.
Nomura H, Furuta A, Suzuki SO, Iwaki T. 2001. Dorsal horn lesion resulting from spinal root avulsion leads to the accumulation of stress-responsive proteins. Brain Res 893:84–94.
Ono K, Han J. 2000. The p38 signal transduction pathway: activation and function. Cell Signal 12:1–13.
Ramer MS, Murphy PG, Richardson PM, Bisby MA. 1998. Spinal nerve lesion-induced mechanoallodynia and adrenergic sprouting in sensory ganglia are attenuated in interleukin-6 knockout mice. Pain 78:115–121.
Scholz J, Woolf CJ. 2002. Can we conquer pain? Nat Neurosci 5(suppl):1062–1067.
Shigemoto-Mogami Y, Koizumi S, Tsuda M, Ohsawa K, Kohsaka S, Inoue K. 2001. Mechanisms underlying extracellular ATP-evoked interleukin-6 release in mouse microglial cell line, MG-5. J Neurochem 78:1339–1349.
Sommer C, Schmidt C, George A. 1998. Hyperalgesia in experimental neuropathy is dependent on the TNF receptor 1. Exp Neurol 151: 138–142.
Sweitzer S, Martin D, DeLeo JA. 2001. Intrathecal interleukin-1 receptor antagonist in combination with soluble tumor necrosis factor receptor exhibits an anti-allodynic action in a rat model of neuropathic pain. Neuroscience 103:529–539.
Tikka T, Fiebich BL, Goldsteins G, Keinanen R, Koistinaho J. 2001. Minocycline, a tetracycline derivative, is neuroprotective against excitotoxicity by inhibiting activation and proliferation of microglia. J Neurosci 21:2580–2588.
Tong L, Pav S, White DM, Rogers S, Crane KM, Cywin CL, Brown ML, Pargellis CA. 1997. A highly specific inhibitor of human p38 MAP kinase binds in the ATP pocket. Nat Struct Biol 4:311–316.
Tsuda M, Mizokoshi A, Shigemoto-Mogami Y, Koizumi S, Inoue K. 2002a. p38 mitogen-activated protein kinase (p38MAPK) is activated in the spinal microglia of neuropathic pain model. Jpn J Pharmacol 88:82.
Tsuda M, Mizokoshi A, Mogami Y, Koizumi S, Inoue K. 2002b. Activation of p38 mitogen-activated protein kinase (p38MAPK) in the spinal microglia in a rat model of neuropathic pain. Soc Neurosci Abs 32:655.14
Tsuda M, Shigemoto-Mogami Y, Koizumi S, Mizokoshi A, Kohsaka S, Salter MW, Inoue K. 2003. $P2X_4$ receptors induced in spinal microglia gate tactile allodynia after nerve injury. Nature (in press).
Watkins LR, Milligan ED, Maier SF. 2001. Spinal cord glia: new players in pain. Pain 93:201–205.
Watkins LR, Martin D, Ulrich P, Tracey KJ, Maier SF. 1997. Evidence for the involvement of spinal cord glia in subcutaneous formalin induced hyperalgesia in the rat. Pain 71:225–235.
Winkelstein BA, Rutkowski MD, Sweitzer SM, Pahl JL, DeLeo JA. 2001. Nerve injury proximal or distal to the DRG induces similar spinal glial activation and selective cytokine expression but differential behavioral responses to pharmacologic treatment. J Comp Neurol 439:127–139.
Woolf CJ, Mannion RJ. 1999. Neuropathic pain: aetiology, symptoms, mechanisms, and management. Lancet 353:1959–1964.
Woolf CJ, Salter MW. 2000. Neuronal plasticity: increasing the gain in pain. Science 288:1765–1769.
Yaksh TL, Jessell TM, Gamse R, Mudge AW, Leeman SE. 1980. Intrathecal morphine inhibits substance P release from mammalian spinal cord in vivo. Nature 286:155–157.

J Pharmacol Sci 94, 112 – 114 (2004)

Journal of Pharmacological Sciences

Forum Minireview

ATP- and Adenosine-Mediated Signaling in the Central Nervous System: Chronic Pain and Microglia: Involvement of the ATP Receptor $P2X_4$

Kazuhide Inoue[1,2,*], Makoto Tsuda[1], and Schuichi Koizumi[3]

Divisions of [1]Biosignaling and [3]Pharmacology, National Institute of Health Sciences, 1-18-1 Kamiyoga, Setagaya-ku, Tokyo 158-8501, Japan

[2]Department of Molecular and System Pharmacology, Graduate School of Pharmaceutical Sciences, Kyushu University, 3-1-1 Maidashi, Higashi-ku, Fukuoka 812-8582, Japan

Received November 7, 2003; Accepted December 2, 2003

Abstract. We have been studying the role of ATP receptors in pain and already reported that activation of $P2X_{2/3}$ heteromeric channel/receptor in primary sensory neurons causes acutely tactile allodynia, one hallmark of neuropathic pain. We report here that tactile allodynia under the chronic pain state requires an activation of the $P2X_4$ ionotropic ATP receptor and p38 mitogen-activated protein kinase (MAPK) in spinal cord microglia. Two weeks after L5 spinal nerve injury, rats displayed a marked mechanical allodynia. In the rats, activated microglia were detected in the injured side of the dorsal horn and the level of the dually-phosphorylated active form of p38MAPK (phospho-p38MAPK) in these microglia was increased. Moreover, intraspinal administration of a p38MAPK inhibitor, SB203580, suppressed the allodynia. We also found that the expression level of $P2X_4$ was increased strikingly in spinal cord microgila after nerve injury and that pharmacological blockade or inhibition of the expression of $P2X_4$ reversed the allodynia. Taken together, our results demonstrate that activation of $P2X_4$ or p38MAPK in spinal cord microglia is necessary for tactile allodynia after nerve injury.

Keywords: ATP receptor, $P2X_4$, microglia, p38 mitogen-activated protein kinase, allodynia

Introduction

Injury of primary sensory neurons produces long-lasting abnormal hypersensitivity to normally innocuous stimuli, a phenomenon known as tactile allodynia (1, 2). Tactile allodynia is the most troublesome of the neuropathic pain syndromes in humans and the mechanisms by which nerve injury develops tactile allodynia have remained unknown (3).

The present article introduces our recent study (4, 5) revealing crucial roles of two molecules, expression and activation of which are highly restricted in microglia in the spinal cord, in neuropathic pain: p38 mitogen-activated protein kinase (p38MAPK) and $P2X_4$ receptor, a subtype of ionotropic ATP receptors.

*Corresponding author (affiliation #1). FAX: +81-3-3700-1349
E-mail: inoue@nihs.go.jp

p38MAPK was activated in spinal hyperactive microglia after nerve injury

Animals with spinal nerve injury displayed tactile allodynia. Paw withdrawal threshold (PWT) (ipsilateral side) to mechanical stimulation significantly decreased at 7 and 14 days. At day 7 and 14, the OX42 labelling was greater in the dorsal horn ipsilateral to the nerve injury. OX42-positive cells were more numerous and displayed hypertrophic morphology in the dorsal horn on the side of the nerve injury as compared with the contralateral side (4). To examine whether p38MAPK is activated in the spinal cord in rats that have developed tactile allodynia, we performed Western blot analysis using an antibody targeting the phosphorylated p38MAPK (phospho-p38MAPK). The band intensity of phospho-p38MAPK protein in the ipsilateral spinal cord dramatically increased 7 and 14 days after nerve injury compared with that in naive rat. Furthermore, we observed strong phospho-p38MAPK immunofluorescence

in the injury side of L5 dorsal spinal cord sections at 7 and 14 days after nerve injury (5). The bilateral difference in phospho-p38MAPK levels parallel with the emergence of the tactile allodynia. These results indicate that the p38MAPK is activated in the dorsal horn ipsilateral to the nerve injury, which may correlate with the nerve injury-induced tactile allodynia. We carried out double immunolabeling for phospho-p38MAPK and for cell type-specific markers to identify the type of cells and found that cells showing phospho-p38MAPK immunofluorescence was double labeled with OX42 but not with neuronal nuclei (NeuN) or glial fibrillary acidic protein (GFAP), indicating that activation of p38MAPK in the dorsal horn is highly restricted to microglia (5). OX42 recognizes the complement receptor type 3 (CR3), expression of which is greatly increased in hyperactive versus resting microglia after nerve injury (4 – 6). These results indicate that nerve injury induced a switch from the resting to the hyperactive phenotype in the population of microglia in the dorsal horn. We found that a marked phosphorylation of p38MAPK is observed in individual microglia in the ipsilateral dorsal horn (3.7-fold as compared with the contralateral side), particularly in hyperactive microglia that dramatically expressed OX42 (4). Therefore, we conclude that in the dorsal horn following nerve injury, hyperactive microglia are the cell type that activates p38MAPK and that the level of p38MAPK phosphorylation is dramatically increased in individual microglia.

p38MAPK activation in the spinal microglia caused development and maintenance of tactile allodynia

We examined whether intrathecal treatment with a potent inhibitor of p38MAPK, SB203580, alters the maintenance and development of tactile allodynia following nerve injury. Catheterized rats were treated with SB203580 (3 nmol/10 μL, n = 13) once at day 7 of the nerve injury. SB203580 treated-rats displayed a marked increase in PWT following nerve injury. When the rats were treated with SB203580 (30 nmol/10 μL, n = 9) once a day during 14 days from 0 day of the nerve injury, SB203580-treated rats showed only a slight decrease in PWT. These results suggest that inhibiting spinal p38MAPK activation in microglia by intrathecal treatment with inhibitor for p38MAPK suppresses the maintenance and development of tactile allodynia following spinal nerve injury.

The role of $P2X_4$ receptor in the tactile allodynia

We tested for the involvement of P2X receptors in the tactile allodynia by using ATP receptor blockers and found that tactile allodynia was reversed by the intrathecal administration of 2',3'-*O*-(2,4,6-trinitrophenyl) adenosine 5'-triphosphate (TNP-ATP) (30 nmol), an antagonist of P2X subtypes $P2X_{1-4}$, on day 7. Intrathecal administration of pyridoxial-phosphate-6-azophenyl-2',4'-disulphonic acid (PPADS), an antagonist of P2X subtypes $P2X_{1,2,3,5,7}$, but not of $P2X_4$, had no effect on either testing day. We observed no alteration in motor behaviour following TNP-ATP administration. These results together indicate that TNP-ATP caused a dose-dependent, reversible inhibition of allodynia on the nerve-injured side without a non-specific effect on motor or sensory functioning. At these intrathecal doses, PPADS is known to suppress nociceptive behaviors caused by intrathecal injection of the $P2X_{1,3}$ agonist α,β-methylene ATP. The lack of effect of PPADS on PWT together with the increase by TNP-ATP indicates that tactile allodynia caused by L5 nerve injury depends upon spinal P2X receptors that are sensitive to TNP-ATP and insensitive to PPADS. The pharmacological profile of these P2Xs is consistent with that of the $P2X_4$ subtype.

We found that $P2X_4$ protein in the ipsilateral spinal cord dramatically increased after L5 nerve injury. The increase in $P2X_4$ was detected as early as day 1 and the highest level was observed on day 14. The time-course of the change in $P2X_4$ level in the spinal cord and the bilateral difference in $P2X_4$ levels match the emergence of the tactile allodynia. We performed immunofluorescence on sections of the L5 spinal dorsal horn to examine the distribution of $P2X_4$. In the spinal cord ipsilateral to the nerve injury, we observed strong, punctate $P2X_4$ immunofluorescence in the dorsal horn on day 14. Furthermore, we found that cells showing $P2X_4$ immunofluorescence were not double-labelled for NeuN or GFAP. Almost all of the $P2X_4$-positive cells were double-labelled with OX42, indicating that $P2X_4$s were expressed in microglia.

Next we examined whether tactile allodynia following nerve injury is critically dependent upon functional $P2X_4$ in hyperactive microglia in the dorsal horn using an antisense oligodeoxynucleotide (ODN) targeting $P2X_4$. The nerve injury-induced allodynia was significantly suppressed in animals treated with $P2X_4$ antisense ODN as compared with that in animals treated with mismatch ODN (4). We also found that the level of $P2X_4$ protein in homogenates from the spinal cord of antisense ODN-treated rats was $32.0 \pm 4.8\%$ less than that of mismatch ODN-treated rats (4). These results indicate that intrathecal treatment with $P2X_4$ antisense ODN suppressed both the tactile allodynia and the increase in $P2X_4$ expression following nerve injury.

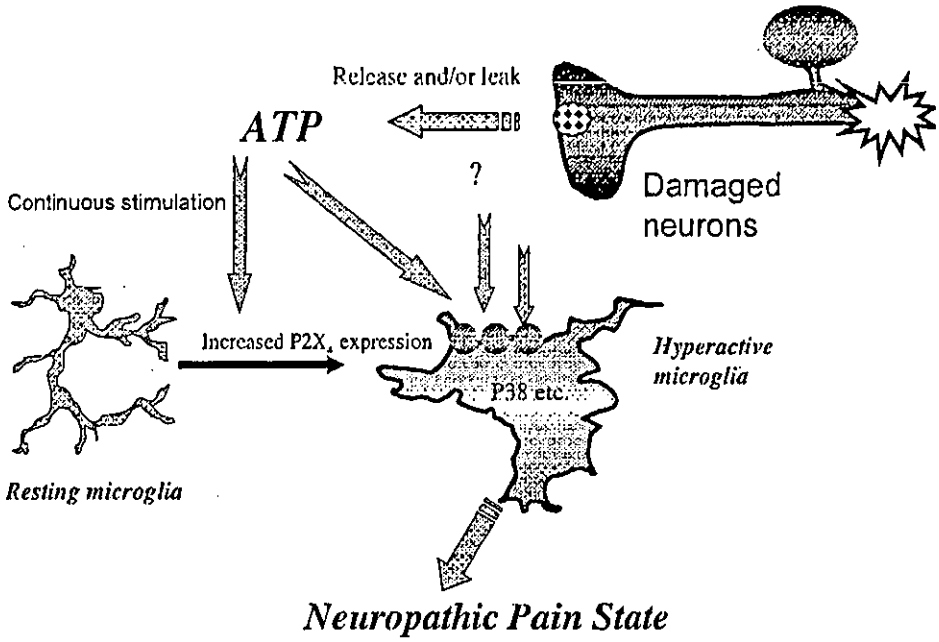

Fig. 1. Hypothesis: neuropathic pain after nerve injury. Tactile allodynia following nerve injury is critically dependent upon functional $P2X_4$ receptors in hyperactive microglia in the dorsal horn. ATP, which might be released or leaked from damaged neurons or astrocytes, stimulates resting microglia to be converted to hyperactive microglia. Hyperactive microglia increases the expression of $P2X_4$ receptors and p38-phosphorelation, resulting in tactile allodynia following nerve injury.

Conclusion

In the present article, we demonstrate that microglia in the spinal dorsal horn are converted to the hyperactive phenotype as a consequence of peripheral nerve injury and have dramatically expressed $P2X_4$ and activated p38MAPK. Also we suggested that the activation of p38MAPK and $P2X_4$ in spinal cord microglia are essential for allodynia after nerve injury (Fig. 1). The allodynia was reversed rapidly by pharmacological blockade of p38MAPK activation or inhibiting the expression of $P2X_4$ receptors, implying that nerve injury-induced pain hypersensitivity depends upon ongoing signaling via $P2X_4$ and/or p38MAPK, likely activated by ATP that may be released from primary sensory terminals (7–9), dorsal horn neurons (7, 10, 11), or dorsal horn astrocytes (12). Inhibition of $P2X_4$ expression, inhibiting the function of these receptors and/or p38MAPK in spinal microglia can be novel therapeutic approaches for treating tactile allodynia caused by nerve damage.

References

1 Woolf CJ, Mannion RJ. Neuropathic pain: aetiology, symptoms, mechanisms, and management. Lancet. 1999;353:1959–1964.
2 Scholz J, Woolf CJ. Can we conquer pain? Nat Neurosci. 2002;5:1062–1067.
3 Woolf CJ, Salter MW. Neuronal plasticity: increasing the gain in pain. Science. 2000;288:1765–1769.
4 Tsuda M, Shigemoto-Mogami Y, Koizumi S, et al. P2X4 receptors induced in spinal microglia gate tactile allodynia after nerve injury. Nature. 2003;424:778–783.
5 Tsuda M, Mizokoshi A, Shigemoto-Mogami Y, Koizumi S, Inoue K. Activation of p38 mitogen-activated protein kinase in spinal hyperactive microglia contributes to pain hypersensitivity following peripheral nerve injury. Glia. 2004;45:89–95.
6 Aldskogius H, Kozlova EN. Central neuron-glial and glial-glial interactions following axon injury. Prog Neurobiol. 1998;55:1–26.
7 Sawynok J, Downie JW, Reid AR, Cahill CM, White TD. ATP release from dorsal spinal cord synaptosomes: characterization and neuronal origin. Brain Res. 1993;610:32–38.
8 Li P, Calejesan AA, Zhuo M. ATP P2X receptors and sensory synaptic transmission between primary afferent fibers and spinal dorsal horn neurons in rats. J Neurophysiol. 1998;80:3356–3360.
9 Nakatsuka T, Gu JG. ATP P2X receptor-mediated enhancement of glutamate release and evoked EPSCs in dorsal horn neurons of the rat spinal cord. J Neurosci. 2001;21:6522–6531.
10 Bardoni R, Goldstein PA, Lee CJ, Gu JG, MacDermott AB. ATP P2X receptors mediate fast synaptic transmission in the dorsal horn of the rat spinal cord. J Neurosci. 1997;17:5297–5304.
11 Jo YH, Schlichter R. Synaptic corelease of ATP and GABA in cultured spinal neurons. Nat Neurosci. 1999;2:241–245.
12 Fam SR, Gallagher CJ, Salter MW. $P2Y_1$ purinoceptor-mediated Ca^{2+} signaling and Ca^{2+} wave propagation in dorsal spinal cord astrocytes. J Neurosci. 2000;20:2800–2808.

Ca^{2+} waves in keratinocytes are transmitted to sensory neurons: the involvement of extracellular ATP and $P2Y_2$ receptor activation

Schuichi KOIZUMI*, Kayoko FUJISHITA†, Kaori INOUE‡, Yukari SHIGEMOTO-MOGAMI†, Makoto TSUDA† and Kazuhide INOUE†§[1]

*Division of Pharmacology, National Institute of Health Sciences, 1-18-1 Kamiyoga, Setagaya, Tokyo 158-8501, Japan, †Division of Biosignaling, National Institute of Health Sciences, 1-18-1 Kamiyoga, Setagaya, Tokyo 158-8501, Japan, ‡Shiseido Research Center, 2-12-1 Fukuura, Kanazawa-ku, Yokohama 236-8643, Japan, and §Graduate School of Pharmaceutical Sciences, Kyushu University, 3-1-1 Maidashi, Fukuoka 812-8582, Japan

ATP acts as an intercellular messenger in a variety of cells. In the present study, we have characterized the propagation of Ca^{2+} waves mediated by extracellular ATP in cultured NHEKs (normal human epidermal keratinocytes) that were co-cultured with mouse DRG (dorsal root ganglion) neurons. Pharmacological characterization showed that NHEKs express functional metabotropic $P2Y_2$ receptors. When a cell was gently stimulated with a glass pipette, an increase in $[Ca^{2+}]_i$ (intracellular Ca^{2+} concentration) was observed, followed by the induction of propagating Ca^{2+} waves in neighbouring cells in an extracellular ATP-dependent manner. Using an ATP-imaging technique, the release and diffusion of ATP in NHEKs were confirmed. DRG neurons are known to terminate in the basal layer of keratinocytes. In a co-culture of NHEKs and DRG neurons, mechanical-stimulation-evoked Ca^{2+} waves in NHEKs caused an increase in $[Ca^{2+}]_i$ in the adjacent DRG neurons, which was also dependent on extracellular ATP and the activation of $P2Y_2$ receptors. Taken together, extracellular ATP is a dominant messenger that forms intercellular Ca^{2+} waves in NHEKs. In addition, Ca^{2+} waves in NHEKs could cause an increase in $[Ca^{2+}]_i$ in DRG neurons, suggesting a dynamic cross-talk between skin and sensory neurons mediated by extracellular ATP.

Key words: ATP, Ca^{2+} wave, cross-talk, dorsal root ganglion neuron, keratinocyte, $P2Y_2$ receptor.

INTRODUCTION

The skin is the largest organ of the body and is exposed to multiple external stimuli. It protects water-rich internal organs from harmful environmental factors such as dryness, chemicals, noxious heat and UV irradiation. In addition, the skin is exposed to various substances such as ATP, bradykinin and histamine after skin injury and during inflammatory skin diseases and allergic reactions respectively. Thus the skin expresses various sensors for environmental stimuli [1,2] or neurotransmitters [3–6]. Various environmental stimuli or neurotransmitters often cause changes in $[Ca^{2+}]_i$ (intracellular Ca^{2+} concentration) in the skin [5,7,8]. Ca^{2+} dynamics play an important role in the homoeostasis of the skin epidermis, the outermost part of skin tissue; the skin epidermis tunes the balance between the proliferation and differentiation of epidermal keratinocytes [1,9].

Propagation of intercellular Ca^{2+} waves from one cell to another is a well-known phenomenon in non-excitable cells such as astrocytes [10,11], hepatocytes [12], epithelial cells [13] and endothelial cells [14]. These cells lack regenerative electrical action potentials but use Ca^{2+} waves for their long-range communications. In astrocytes, extracellular molecules such as glutamate [11] and ATP [15], rather than gap junction via connexin43, have been suggested to be important factors for the Ca^{2+} wave [16]. Epidermal keratinocytes are non-excitable cells and do not produce action potentials. However, the mechanisms of intercellular Ca^{2+} waves in keratinocytes have received only limited attention. Given that Ca^{2+} waves in keratinocytes are mediated by the release of extracellular molecules, such signals may also affect the activity of surrounding cells such as sensory neurons. Although junctions have not been found between keratinocytes and sensory termini, ultrastructural studies have shown that keratinocytes contact DRG (dorsal root ganglion) nerve fibres through membrane–membrane apposition [17,18]. Immunostaining of the neuronal marker PGP 9.5 (protein gene product 9.5) revealed the presence of free nerve endings at epidermal keratinocytes [19]. There is indirect evidence that keratinocytes communicate with sensory neurons via extracellular molecules. For example, although dissociated DRG neurons can be directly activated by heat and cold, warm responses have only been demonstrated in experiments where skin–nerve connectivity is intact [20,21]. A warmth sensor, TRPV3, is present in epidermal keratinocytes, but not in sensory neurons [19]. Sensory neurons themselves sense various external stimuli, but there might be skin-derived regulatory mechanisms by which sensory signalling is modulated.

In the present study, we report that mechanical stimulation of NHEKs (normal human epidermal keratinocytes) with a glass pipette induces propagating Ca^{2+} waves in an extracellular ATP-dependent manner. NHEKs release ATP and, in turn, the released ATP activates $P2Y_2$ receptors in NHEKs. We also demonstrate that, in a co-culture of NHEKs and DRG neurons, such extracellular ATP-dependent Ca^{2+} waves in NHEKs cause increases in $[Ca^{2+}]_i$ even in the adjacent DRG neurons, suggesting that dynamic cross-talk occurs between keratinocytes and DRG neurons via extracellular ATP.

EXPERIMENTAL

Cell culture

NHEKs were obtained as cryopreserved first passage cells from neonatal foreskins (Kurabo, Osaka, Japan). Cells were plated on collagen-coated coverslips and then cultured in serum-free

Abbreviations used: ATPγS, adenosine 5′-[γ-thio]triphosphate; BSS, balanced salt solution; $[Ca^{2+}]_i$, intracellular Ca^{2+} concentration; DRG, dorsal root ganglion; αβmeATP, α,β-methylene-ATP; 2meSADP, 2methyl-thio-ADP; NHEK, normal human epidermal keratinocyte; RT, reverse transcriptase.

[1] To whom correspondence should be addressed (e-mail inoue@nihs.go.jp).

keratinocyte growth medium consisting of Humedia-KB2 (Kurabo), supplemented with bovine pituitary extract (0.4 %, v/v), human recombinant epidermal growth factor (0.1 ng/ml), insulin (10 μg/ml), cortisol (0.5 μg/ml), gentamicin (50 μg/ml) and amphotericin B (50 ng/ml). The media were replaced every 2–3 days. For co-culturing NHEKs and mouse DRG neurons, NHEKs were seeded on mitomycin C (4 μg/ml)-treated 3T3-J2 fibroblast feeder layers (2×10^5 cells/cm^2) in 'Green' medium [3:4 Dulbecco's minimal Eagle's medium and 1:4 Ham's F12, supplemented with 10 % (v/v) foetal bovine serum, 20 mM Hepes, 100 units/ml penicillin, 100 μg/ml streptomycin, 5 μg/ml insulin, 0.5 μg/ml cortisol, 0.1 nM cholera enterotoxin, 0.01 μg/ml recombinant human epidermal growth factor, 0.25 μg/ml amphotericin B and 180 μM adenine]. The dissociated mouse DRG neurons were seeded, 2 days after the seeding of NHEKs, on the cell layer and then cultured for an additional 1 week.

Ca^{2+} imaging in single NHEKs

Changes in $[Ca^{2+}]_i$ in single cells were measured by the fura 2 method as described by Grynkiewicz et al. [22] after minor modifications [23]. In brief, the culture medium was replaced with BSS (balanced salt solution) of the following composition (mM): NaCl 150, KCl 5.0, $CaCl_2$ 1.8, $MgCl_2$ 1.2, Hepes 25 and D-glucose 10 (pH 7.4). Cells were loaded with fura 2 by incubation with 5 μM fura 2/AM (fura 2 acetoxymethyl ester; Molecular Probes, Eugene, OR, U.S.A.) at room temperature (20–22 °C) in BSS for 45 min, followed by washing with BSS and a further 15 min incubation to allow de-esterification of the loaded dye. The coverslips were mounted on an inverted epifluorescence microscope (TMD-300; Nikon, Tokyo, Japan) equipped with a 75 W xenon lamp and band-pass filters of 340 and 360 nm wavelengths. Measurements were carried out at room temperature. Images were recorded by a high-sensitivity silicon intensifier target camera (C-2741-08; Hamamatsu Photonics, Hamamatsu, Japan) and the image data were regulated by a Ca^{2+} analysing system (Furusawa Laboratory Appliance, Kawagoe, Japan). The absolute $[Ca^{2+}]_i$ was estimated from the ratio of emitted fluorescences (F_{340}/F_{360}) according to a calibration curve obtained by using Ca^{2+} buffers. For Ca^{2+}-free experiments, Ca^{2+} was removed from the BSS (0 Ca^{2+}). Drugs were dissolved in BSS and applied by superfusion. For mechanical stimulation, a single NHEK in the centre of the microscopic field was probed with a glass micropipette using a micromanipulator (Narishige, Tokyo, Japan). Under visible light, the tip of the micropipette was positioned approx. 2 μm over the cell to be stimulated. When sampling, the micropipette was rapidly lowered by approx. 2 μm and then rapidly returned to its original position. If the stimulated cell showed no increase in fluorescence, the pipette was lowered again until stimulation was seen. If the stimulated cell showed any sign of damage (dye leakage or abnormal morphology), the experiment was eliminated. For confocal Ca^{2+} imaging, the cells were loaded with 5 μM fura 4/AM for 30–40 min at room temperature and then mounted on a microscope (TE-2000; Nikon) equipped with a CSU-10 laser-scanning unit (Yokogawa, Tokyo, Japan) and a high-sensitivity CCD (charge-coupled-device) camera (ORCA-ER; Hamamatsu Photonics), as described previously [24]. To compensate for the uneven distribution of the fluo-4, self-ratios were calculated ($R_s = F/F_0$), which were subsequently converted into Ca^{2+} concentration using the following equation:

$$[Ca^{2+}]_i = R_s K_d / [(K_d / [Ca^{2+}]_{rest}) - R_s]$$

The K_d value of fluo-4 for NHEKs was taken to be 706 nM as determined by an *in vivo* calibration method.

Table 1 Primer pairs and end-products

Amplicon shows the base pairs of the PCR end-product.

Gene	Primer	Size (-mer)	Amplicon (bp)
P2Y1	F: 5′-GAGGGCCCGGCTTGATT-3′	17	67
	R: 5′-ATACGTGGCATAAACCCTGTCA-3′	22	
P2Y2	F: 5′-TGGTGCGCTTCCTCTTCTACA-3′	21	72
	R: 5′-ACCGGTGCACGCTGATG-3′	17	
P2Y4	F: 5′-TCATGGCTCGTCGCCTGTA-3′	19	67
	R: 5′-AGAGAGCGGAGGCGAGAAG-3′	19	
P2Y6	F: 5′-CCTGCCCACAGCCATCTT-3′	18	116
	R: 5′-CAGTGAGAGCCATGCCATAGG-3′	21	
P2Y11	F: 5′-CTGCCCTGCCAACTTCTTG-3′	19	78
	R: 5′-ACCAGTATGGGCCACAGGAA-3′	20	
P2Y12	F: 5′-CCTTTCCATTTTGCCCGAAT-3′	20	74
	R: 5′-GTATTTTCAGCAGTGCAGTCAAAGA-3′	25	

Imaging of ATP release

ATP release from NHEKs was detected with a luciferin–luciferase bioluminescence assay. After an initial 30 min superfusion period, superfusion was stopped and the cell chamber was filled with BSS containing a luciferase reagent (ATP bioluminescence assay kit CLS II; Roche Diagnostics, Mannheim, Germany). ATP bioluminescence was detected and visualized with a VIM camera (C2400-35; Hamamatsu Photonics) using an integration time of 30 s. The absolute ATP concentration was estimated using a standard ATP solution (ATP bioluminescence assay kit CLS II).

Immunocytochemistry

Cultures were fixed with 4 % (w/v) paraformaldehyde for 10 min and soaked in PBS solution. Cells were incubated with primary antibodies (rabbit anti-peripherin antibody, 1:200; Chemicon, Temecula, CA, U.S.A.; monoclonal mouse anti-cytokeratin14 antibody, 1:100; Cymbus Biotechnology, Chandlers Ford, U.K.), dissolved in blockace solution (1:10 dilution; Dainippon, Osaka, Japan) for 1 h at room temperature and then covered with diluted (1:500) secondary fluorescent antiserum solution (Alexa488- and Alexa546-conjugated rabbit and mouse anti-IgGs respectively) and kept at 4 °C overnight. Then, the cells were washed three times with PBS containing 0.05 % Tween 20 for 15 min and mounted with Vectashied (Vector Laboratories, Burlingame, CA, U.S.A.). Images were obtained by confocal microscopy (Radiance 2000; Bio-Rad Japan, Tokyo, Japan).

Reverse transcriptase (RT)–PCR of P2 receptors

The total RNA was isolated and purified using RNeasy mini kits (Qiagen) according to the manufacturer's instructions. RT–PCR amplifications were performed using Taqman One-step RT–PCR Master Mix Reagents and 200 nM of each P2 receptor-specific primer. Using the software Primer Express (Applied Biosystems, Tokyo, Japan), clone-specific primers were designed to recognize human P2Y receptors, as shown in Table 1. All primers had similar melting temperatures for running the same cycling programme for all samples. RT–PCR was performed by 30 min reverse transcription at 48 °C, 10 min AmpliTaq Gold activation at 95 °C, then 15 s denaturation at 95 °C and, finally, 1 min annealing and elongation at 60 °C for 40 cycles in a PRISM 7700 (Applied Biosystems). To exclude contamination by unspecific PCR products such as primer dimers, melting curve analysis was performed on all the final PCR products after the cycling procedure.

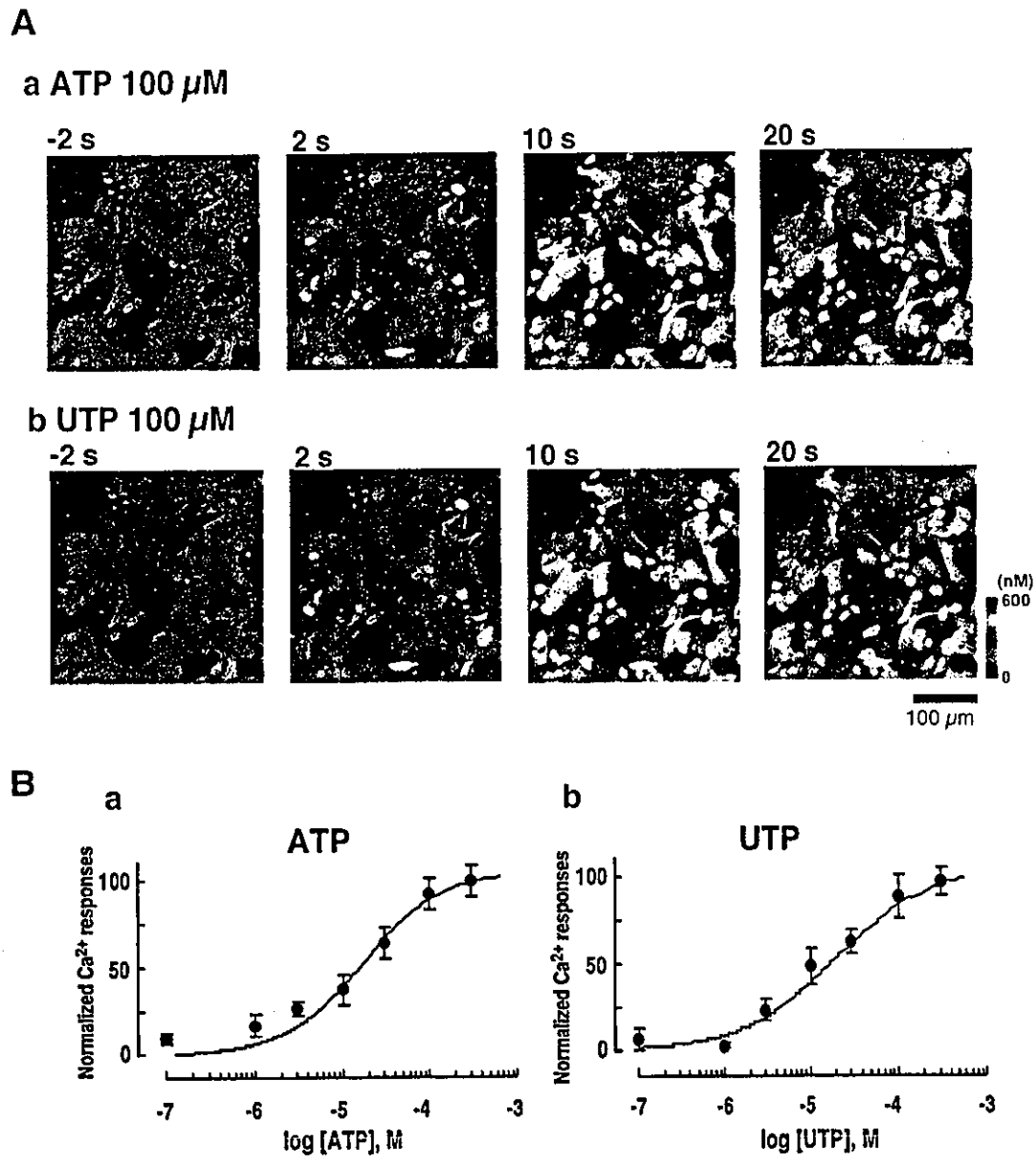

Figure 1 Increases in $[Ca^{2+}]_i$ evoked by both applied ATP and UTP in NHEKs

(A) Sequential pseudo colour images of Ca^{2+} responses to 100 μM ATP (a) and UTP (b). Images were obtained from a confocal laser microscope, showing self-ratios of fluo-4 fluorescence. Images were recorded 2 s before (−2 s) and 2, 10 and 20 s after ATP or UTP application. (B) Concentration–response curves for (a) ATP- and (b) UTP-evoked increases in $[Ca^{2+}]_i$ in NHEKs. Increases in $[Ca^{2+}]_i$ in NHEKs were monitored by ratiometric fura 2 fluorescence ($\Delta F_{340}/F_{360}$) and were then converted into absolute value of $[Ca^{2+}]_i$ using a standard calibration curve. The maximum $[Ca^{2+}]_i$ increase was observed when cells were stimulated with 300 μM ATP (a) or UTP (b). The increase in $[Ca^{2+}]_i$ at each ATP or UTP concentration was normalized by the maximum increase in $[Ca^{2+}]_i$. Results are the means ± S.E.M. for 28–73 cells tested. Both the ATP- and UTP-evoked concentration–response curves were almost identical with the ED_{50} values of 21 and 20 μM respectively.

Statistics

Experimental results are expressed as means ± S.E.M. and statistical differences between two groups were determined by Student's *t* test.

RESULTS

Characterization of ATP-evoked $[Ca^{2+}]_i$ increases in NHEKs

Exogenously applied ATP induced an increase in $[Ca^{2+}]_i$ in NHEKs with an ED_{50} value of 21 μM (Figures 1Aa and 1Ba). UTP also caused an increase in $[Ca^{2+}]_i$ in the cells, with a similar ED_{50} value of 20 μM (Figures 1Ab and 1Bb). The ATP-evoked increase in $[Ca^{2+}]_i$ was almost independent of the extracellular Ca^{2+}, but was decreased by U73122, an inhibitor of phospholipase C, and thapsigargin, an inhibitor of Ca^{2+}-ATPase of Ca^{2+} stores, suggesting the involvement of inositol 1,4,5-trisphosphate/phospholipase C-linked metabotropic P2Y receptors in the Ca^{2+} responses (Figure 2A). UTP activates UTP-preferring $P2Y_2$ and $P2Y_4$ receptors, and UDP, generated by de-phosphorylation of UTP, stimulates $P2Y_6$ receptors. We therefore analysed the expression of mRNAs for these P2Y receptors using an RT–PCR method and detected the signals for $P2Y_1$, $P2Y_2$ and $P2Y_{11}$ receptors (Figure 2B, inset). Each PCR product possessed the predicted length (Table 1). Signals for $P2Y_4$, $P2Y_6$ and $P2Y_{12}$ were hardly detected in NHEKs. To confirm the functional responses

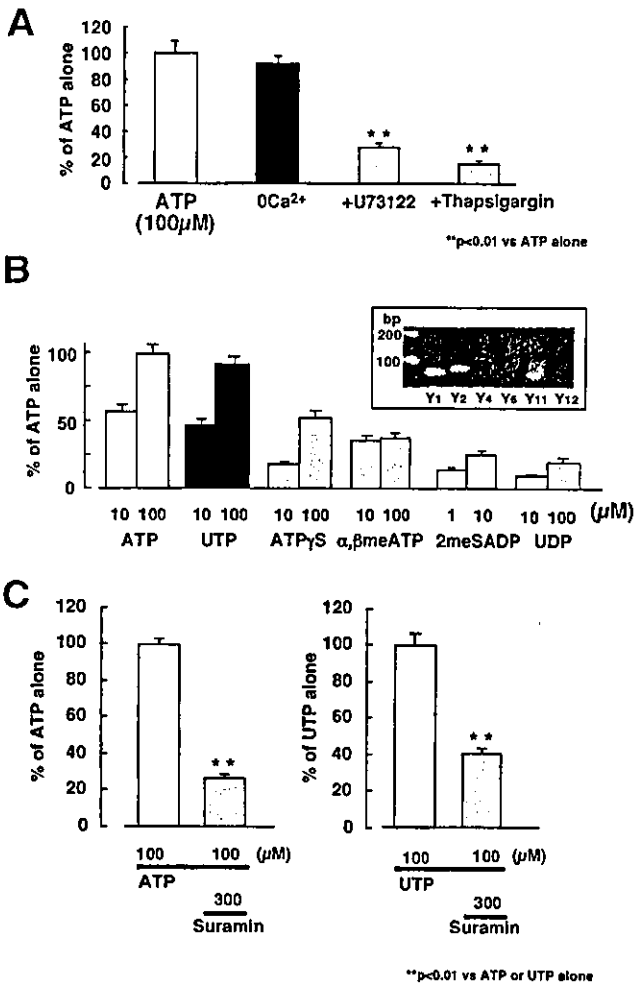

Figure 2 Characterization of P2 receptor-mediated Ca^{2+} responses in NHEKs

The ATP-evoked increases in $[Ca^{2+}]_i$ in NHEKs were characterized. Increases in $[Ca^{2+}]_i$ in cells were calculated by ratiometric fura 2 fluorescence ($\Delta F_{340}/F_{360}$) and a standard calibration curve. Values were normalized by the Ca^{2+} response at 100 μM ATP or UTP and were expressed as a percentage of ATP or UTP alone (**C**, right). (**A**) ATP was applied to NHEKs for 20 s and the U73122 (5 μM) was applied to the cells 10 min before and during the ATP application. Thapsigargin (100 nM) was applied to the cells 5 min before and during the ATP application. Results were obtained from 28 to 61 cells tested (at least two independent experiments). $^{**}P < 0.01$, significant differences from the response evoked by ATP alone. (**B**) Pharmacological characterization of Ca^{2+} responses in NHEKs. UTP was as potent as ATP. ATPγS and $\alpha\beta$meATP were much less potent than ATP. 2meSADP and UDP caused only slight increases in $[Ca^{2+}]_i$ in NHEKs. Results were obtained from 24 to 57 cells tested (at least two independent experiments). The inset shows the agarose-gel electrophoresis, indicating expression of mRNAs for various P2Y receptors in NHEKs. (**C**) Suramin (300 μM) inhibited both the ATP- and UTP-evoked increases in $[Ca^{2+}]_i$ in NHEKs. Results were obtained from 117 to 128 cells tested (four independent experiments). $^{**}P < 0.01$, significant differences from the response evoked by ATP or UTP alone.

of these P2Y receptors, we further performed pharmacological analysis using the fura 2-based Ca^{2+} imaging methods. The increase in $[Ca^{2+}]_i$ evoked by UTP was almost identical with that evoked by ATP. Both the $P2Y_{11}$ receptor agonist ATPγS (adenosine 5′-[γ-thio]triphosphate) and the P2X receptor agonist $\alpha\beta$meATP (α,β-methylene-ATP) caused increases in $[Ca^{2+}]_i$, but they were less than those caused by ATP or UTP. 2meSADP (2methyl-thio-ADP), a $P2Y_1$ receptor agonist, and UDP, a $P2Y_6$ receptor agonist, evoked only slight increases in $[Ca^{2+}]_i$ in the cells. The potency rank order for the Ca^{2+} response was ATP = UTP > ATPγS > $\alpha\beta$meATP > 2meSADP > UDP (Figure 2B). Cross-desensitization was observed between ATP and UTP (results not shown). Suramin at 300 μM decreased both the ATP- and UTP-evoked $[Ca^{2+}]_i$ increases (Figure 2C: 29.8 ± 2.2 % of ATP alone, $n = 128$; 44.1 ± 2.7 % of UTP alone, $n = 117$). These results suggest that the $P2Y_2$ receptors were responsible for these responses.

Propagating Ca^{2+} waves in response to mechanical stimulation in NHEKs

When an NHEK was stimulated with a glass pipette, an increase in $[Ca^{2+}]_i$ in the cell was observed, followed by induction of a propagating Ca^{2+} wave after a time lag in neighbouring NHEKs (Figure 3A, upper panels). The findings that the same cell evoked a Ca^{2+} response to repeated (up to three times) mechanical stimulations (results not shown) and that the cell showed some sign of damage suggest that mechanical stimulation would not cause injury to the stimulated cells. The propagation of Ca^{2+} waves was abolished by 80 units/ml apyrase [grade III; Figures 3A (lower panels) and 3B]. Both the P2 receptor antagonists suramin (300 μM) and pyridoxal phosphate-6-azophenyl-2′,4′-disulphonic acid (100 μM) significantly inhibited the Ca^{2+} wave; however, adenosine 3′-phosphate 5′-phosphosulphate (100 μM), an antagonist to the $P2Y_1$ receptor, and 1-octanol (500 μM), an inhibitor of gap junction, did not affect the Ca^{2+} waves (Figure 3C). The $[Ca^{2+}]_i$ increase in the stimulated cells was not affected by these antagonists. All these findings suggest that the propagating Ca^{2+} wave in response to mechanical stimulation in NHEKs was mediated by extracellular ATP and mainly by the activation of $P2Y_2$ receptors.

Release and diffusion of ATP from NHEKs

To demonstrate directly the stimulus-evoked release of ATP from NHEKs, we modified the luciferin–luciferase chemiluminescence bioassay for detecting ATP levels by using a high-sensitivity single photon-counting camera to correlate photon counts with increases in extracellular ATP. NHEKs were bathed in a solution containing the luciferin–luciferase reagents and photons were counted before and 30 s after mechanical stimulation of an NHEK. Figure 4(a) shows a phase-contrast image of a microscopic field, and Figures 4(b) and 4(c) show bioluminescence images before and after mechanical stimulation in the same field respectively. The standard calibration curve obtained under this condition showed a high correlation between the bioluminescence intensity and the ATP concentration with a correlation coefficient of 0.986 over a concentration range of 10 nM–10 μM (Figure 4d). The resting level of the bioluminescence signal was very low; then, it was increased to a level sufficient to evoke increases in $[Ca^{2+}]_i$ in NHEKs (3.2 ± 0.91 μM, $n = 12$) in response to mechanical stimulation for 30 s (Figures 4c and 4f). To visualize the spatiotemporal dynamics of the stimulus-evoked release of ATP from NHEKs, the extracellular ATP levels were plotted as pseudo colour images using the Excel 2-D surface plot program. As shown in Figures 4(e) and 4(f), the levels of extracellular ATP after mechanical stimulation were highest at the site of stimulation and decreased concentrically. These results show that the mechanically evoked Ca^{2+} waves were well associated with the release of ATP from NHEKs and the activation of $P2Y_2$ receptors.

Ca^{2+} waves in NHEKs activate increase in $[Ca^{2+}]_i$ in DRG neurons

As described in the Introduction section, sensory neurons terminate in the skin. Hence, a co-culture of NHEKs and mouse

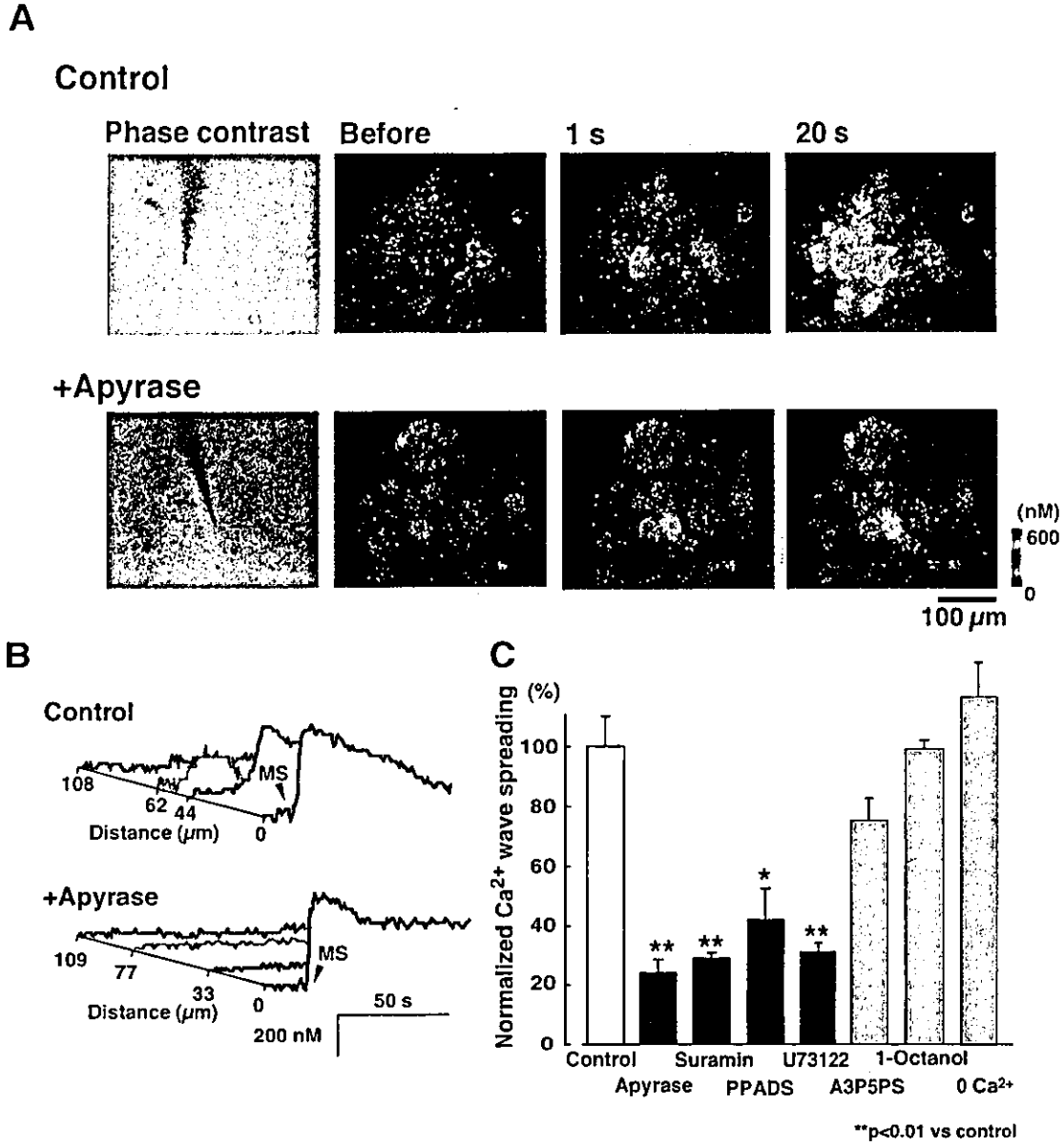

Figure 3 Propagation of Ca^{2+} waves in response to mechanical stimulation in NHEKs

(**A**) Phase-contrast (left) and pseudo $[Ca^{2+}]_i$ images of a field of cultured NHEKs in the absence (upper panels) and presence (lower panels) of apyrase (80 units/ml). Increase in $[Ca^{2+}]_i$ was estimated by ratiometric fura 2 fluorescence ($\Delta F_{340}/F_{360}$) and was then converted into absolute $[Ca^{2+}]_i$ using a standard calibration curve. A single NHEK was mechanically stimulated. (**B**) Plots of $[Ca^{2+}]_i$ as a function of time in four individual NHEKs in the microscopic field. The plots for the non-stimulated cells (blue, green and red traces) horizontally regressed in proportion to their distance from the stimulated cell (black traces) as indicated by the scale bar. In a control experiment, mechanical stimulation of NHEK 1 (black trace) resulted in the induction of a Ca^{2+} wave in adjacent cells after a time lag (upper traces). However, in the presence of apyrase (80 units/ml), mechanical stimulation failed to cause increases in $[Ca^{2+}]_i$ in the surrounding NHEKs (lower traces). The diameter of the spreading distance of the Ca^{2+} wave was calculated in the absence and presence of various chemicals and is summarized in (**C**). The average diameter of the Ca^{2+} wave under the control condition was 93.4 ± 9.7 μm ($n = 12$). Suramin (300 μM), pyridoxal phosphate-6-azophenyl-2′,4′-disulphonic acid (PPADS; 100 μM) and U73122 (5 μM) also abolished the propagation of Ca^{2+} waves, but adenosine 3′-phosphate 5′-phosphosulphate (A3P5PS; 100 μM), 1-octanol (500 μM) or removal of extracellular Ca^{2+} (0 Ca^{2+}) failed to inhibit the mechanical-stimulation-evoked Ca^{2+} wave in NHEKs ($n = 8$–12).

DRG neurons was prepared as described in the Experimental section. Figure 5(A) shows an immunohistochemical image of anti-cytokeratin14 (red) and anti-peripherin (green) antibodies, which are markers for the basal layer of keratinocytes and small-sized DRG neurons respectively. When stimulated with 80 mM KCl, almost all peripherin-positive DRG neurons (Figure 5B, green traces) exhibited increases in $[Ca^{2+}]_i$, whereas cytokeratin14-positive NHEKs (Figure 5B, red trace) did not. Both ATP (100 μM) and UTP (100 μM) caused increases in $[Ca^{2+}]_i$ in 71 % of the small-sized DRG neurons (37 out of 52 cells tested; $dF/F_0 = 6.3 \pm 0.8$ for ATP and 5.8 ± 0.6 for UTP; $n = 37$ in four separate experiments), and 73 % of NHEKs (58 out of 79 cells tested; $dF/F_0 = 5.1 \pm 0.7$ for ATP and 4.3 ± 0.4 for UTP; $n = 58$ in four separate experiments). The UTP-evoked increases in $[Ca^{2+}]_i$ in both types of cells were reproducible, and the first and second UTP-evoked responses were almost identical. The average diameter of the small-sized DRG neurons was 21.8 ± 3.5 μm. Suramin (100 μM) inhibited the UTP-evoked increases in $[Ca^{2+}]_i$ in both types of cells (DRG neurons, 10.2 ± 2.1 % of UTP alone, $n = 37$; NHEKs, 32.1 ± 4.6% of UTP alone, $n = 58$). Thus

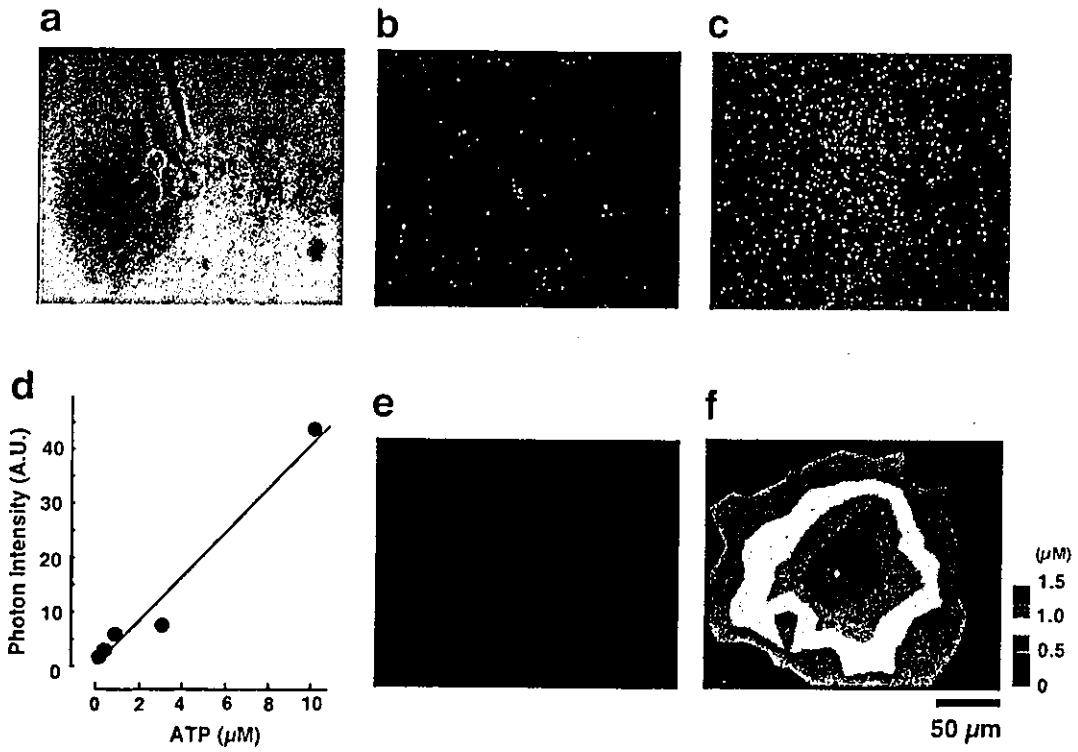

Figure 4 Visualization of release of ATP from NHEKs

The images show photon counts (yellow dots) in a field of NHEKs bathed in luciferin–luciferase reagent before (**b**) and after (**c**) mechanical stimulation. The position of pipette is shown in a phase-contrast image of NHEKs (**a**). (**d**) A typical bioluminescence intensity–ATP concentration relationship under these conditions. Various concentrations of ATP standard solution were injected in the presence of the luciferin–luciferase reagent, and photons were then accumulated for 30 s. (**e**, **f**) Spatial distribution of photon counts of mechanical stimulation shown as a two-dimensional pseudo colour surface plot. Scale bar, 50 μm for images **a**–**c**.

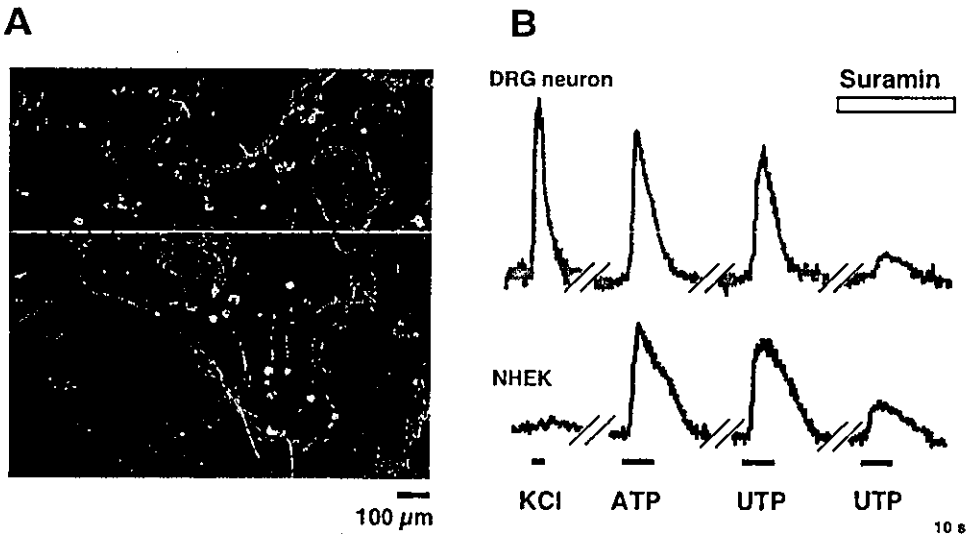

Figure 5 Immunohistochemical staining of DRG neurons and NHEKs

(**A**) After some Ca^{2+} imaging experiments, cells were fixed and stained with anti-cytokeratin14 and anti-peripherin antibodies for confirming NHEKs and small-sized DRG neurons respectively. (**B**) Representative Ca^{2+} responses obtained from self-ratios of fluo-4 fluorescence in anti-peripherin-positive DRG neuron (green) and anti-cytokeratin14-positive NHEK (red). First, cells were stimulated with 80 mM KCl for 3 s. Then, they were stimulated with 100 μM ATP for 10 s and 100 μM UTP for 10 s separated by 5 min. Finally, UTP (100 μM) was applied to the cells in the presence of 100 μM suramin. Both ATP and UTP caused increases in $[Ca^{2+}]_i$ in approx. 71 % of the DRG neurons (37 out of 52 cells tested) and in 73 % of the NHEKs (58 out of 79 cells tested) in the co-cultured cells.

most of the small-sized neurons also expressed UTP-preferring suramin-sensitive P2Y receptors, presumably $P2Y_2$ receptors. In the co-culture of NHEKs and DRG neurons, mechanical stimulation of a single NHEK produced a propagating Ca^{2+} wave in adjacent NHEKs in an extracellular ATP-dependent manner (Figure 6A). Interestingly, this Ca^{2+} wave in the NHEKs was

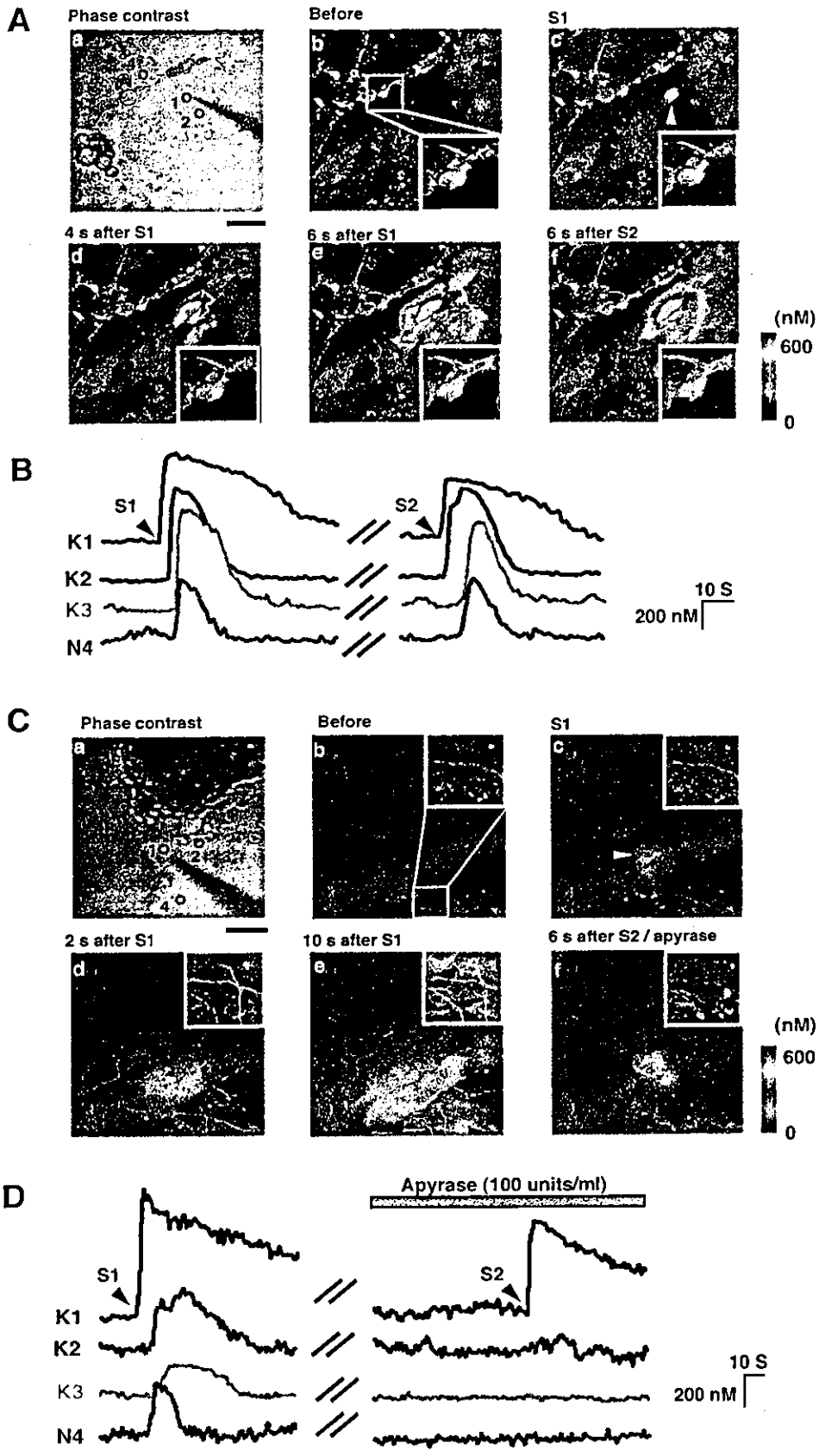

Figure 6 For legend see next page

followed by an increase in $[Ca^{2+}]_i$ in the DRG neurons after a time lag (Figures 6Ae and 6B, trace N4). The increases in $[Ca^{2+}]_i$ in DRG neurons were also dependent on extracellular ATP and the activation of P2 receptors, since the ATP-degrading enzyme, apyrase (grade III, 100 units/ml; Figures 6Cf and 6D), and suramin (100 μM) inhibited the increase in $[Ca^{2+}]_i$ (apyrase, $9.6 \pm 0.9\%$ of S1, $n=21$; suramin, $14.8 \pm 1.9\%$ of S1, $n=33$). Thus we concluded that the release of ATP in response to mechanical stimulation from NHEKs functions as an intercellular molecule between NHEKs and DRG neurons, which may affect nociceptive transduction in peripherin-positive neurons.

DISCUSSION

In the present study, we have demonstrated that ATP is a dominant extracellular signalling molecule in the formation of intercellular Ca^{2+} waves in NHEKs. We also showed that extracellular ATP-dependent Ca^{2+} waves in NHEKs caused increases in $[Ca^{2+}]_i$ in the adjacent DRG neurons. Thus ATP derived from NHEKs functions in both an autocrine and paracrine manner in the peripheral skin-to-sensory neuron system.

Both ATP and UTP caused increases in $[Ca^{2+}]_i$ in NHEKs to a similar extent. These Ca^{2+} responses were independent of extracellular Ca^{2+}, but dependent on inositol 1,4,5-trisphosphate-sensitive Ca^{2+} stores, suggesting the involvement of metabotropic P2Y receptors in the responses. ATP and UTP are natural ligands at $P2Y_2$ receptors, and are approximately equipotent. UTP also activates $P2Y_4$ receptors, but the human $P2Y_4$ receptor is highly selective for UTP than ATP [25]. UDP, an agonist to $P2Y_6$ receptors, only slightly increased the $[Ca^{2+}]_i$ in NHEKs [26,27]. Suramin moderately antagonizes human $P2Y_2$ receptors but not human $P2Y_4$ receptors [28]. NHEKs expressed a large amount of mRNAs for $P2Y_2$ receptors, but not for $P2Y_4$ or $P2Y_6$ receptors. All these pharmacological profiles showed that these responses should be mediated by $P2Y_2$ receptors (Figure 2). Very recently, Greig et al. [29] have reported that skin cells express P2X5, P2X7, $P2Y_1$ and $P2Y_2$ receptors, each of which is expressed in a spatially distinct zone of the epidermis and has distinct cellular functions. $P2Y_2$ receptors are expressed in the lower layer of the epidermis and are involved in proliferation, suggesting that the NHEKs used in the present study might mimic the basal cellular layer of skin cells *in vivo*.

The question remains as to whether endogenous ATP may produce propagating Ca^{2+} waves in NHEKs. Several reports have shown that mechanical stimulation produces a propagating Ca^{2+} wave in non-excitable cells such as astrocytes [15,30] and hepatocytes [12]. In astrocytes, extracellular molecules such as glutamate [11,31] and ATP [15,30], rather than gap junctions [32], are responsible for the propagation of Ca^{2+} waves. We sought to determine whether extracellular ATP produces intercellular Ca^{2+} waves in NHEKs. Mechanical stimulation of a single NHEK resulted in the induction of an intercellular Ca^{2+} wave, which was inhibited by the ATP-degrading enzyme, apyrase, and the P2 receptor antagonist, suramin (Figure 3). The gap junction inhibitor, 1-octanol, had little effect on the Ca^{2+} wave. Imaging of the ATP release by the modified luciferin–luciferase chemiluminescence clearly showed that the levels of extracellular ATP after mechanical stimulation were highest at the site of stimulation and decreased concentrically. These results strongly suggest that the mechanically evoked Ca^{2+} waves in NHEKs are mediated by extracellular ATP and by the activation of $P2Y_2$ receptors. As in astrocytes [15,30], extracellular ATP appears to play a pivotal role in creating the dynamic changes for long-range signalling in NHEKs.

The responses mediated by $P2Y_2$ receptors are probably layer-specific. The ATP-evoked hyperpolarization is very high in the basal layer but extremely low in the suprabasal layer in HaCaT keratinocytes [33]. The mRNA level of $P2Y_2$ receptors is down-regulated in differentiating HaCaT cells [34]. Thus the intercellular Ca^{2+} waves seen in the present study may be a response restricted to the basal layer of keratinocytes *in situ*. The finding that the barrier recovery rate of the mouse epidermis is regulated by functional P2 × 3 [35] suggests that the skin expresses multiple P2 receptors that are linked to distinct physiological functions.

There is an increasing body of evidence that ATP, the predominant extracellular signalling molecule of astrocytes [15,30], may also mediate signalling between neurons and glial cells [36–38]. With regard to the skin-to-sensory neuron system, a similar relationship may also be obtained. Especially, non-myelinated small-sized DRG neurons (nociceptors) terminate in the periphery as free nerve endings [39]. Thus nociceptors can directly contact skin-derived extracellular molecules when skin cells are injured, inflamed or otherwise stimulated. When cells are injured or destroyed, very high concentrations of intracellular ATP (> 5 mM) could leak and affect the surrounding NHEKs and DRG neurons. In the present study, however, we showed that the intercellular Ca^{2+} waves in NHEKs were reproducible when the same cell was stimulated repeatedly (Figure 6). Moreover, the increases in neuronal $[Ca^{2+}]_i$ in response to mechanical stimulation of NHEKs were also reproducible. Thus it appears that extracellular ATP-mediated NHEK-to-DRG neuron communication takes place even when cell damage is not involved. Somatic sensation requires the conversion of physical stimuli into depolarization of the distal nerve endings. It has been reported that activation of $P2Y_1$ receptors in sensory fibres increases the frequency of spikes evoked by a light touch of the skin [40]. Therefore the skin might sense and transmit non-harmful stimuli to sensory neurons via ATP.

DRG neurons express various types of P2 receptors. Ionotropic P2X receptors, especially P2X3 [41] and P2X2 [42] receptors in small- and middle-sized DRG neurons respectively, have been extensively studied in relation to pain. However, recent reports suggest that some P2Y receptors are present in small-sized DRG neurons and are involved in pain signalling. In small-sized neurons, activation of $P2Y_1$ or $P2Y_2$ receptors sensitizes TRPV1 receptors via protein kinase C-dependent mechanisms [43], stimulation of $P2Y_2$ receptors enhances the $[Ca^{2+}]$ increase, leading to the release of CGRP [44], and activation of $P2Y_2$

Figure 6 Dynamic communication between NHEKs and DRG neurons mediated by extracellular ATP

(**A**) Phase-contrast image (**a**) and pseudo colour $[Ca^{2+}]_i$ images (self-ratios of fluo-4 fluorescence; **b–f**) in co-cultured NHEKs and DRG neurons obtained by confocal laser microscopy. The white rectangle field in the middle of image **b** is shown enlarged in the bottom right of images **b–f**. The red arrowhead in image **b** depicts position 4 (DRG neuron 4). The white arrowhead in image **c** shows the initiation of Ca^{2+} wave in response to mechanical stimulation (cell 1). Scale bar, 50 μm. (**B**) The graph shows individual traces of the self-ratios of fluo-4 fluorescence in keratinocytes (K1–K3) and DRG neuron (N4) shown in image **Aa**. Keratinocyte 1 was mechanically stimulated twice (arrows S1 and S2) separated by 5 min. (**C**) Phase-contrast image (**a**) and pseudo colour $[Ca^{2+}]_i$ images (self-ratios of fluo-4 fluorescence; **b–f**) in co-cultured NHEKs and DRG neurons. The white rectangle field in the middle of image **b** is shown enlarged in the top right of images **b–f**. The red arrowhead in image **b** depicts position 4 (DRG neuron 4). The white arrowhead in image **c** shows the initiation of Ca^{2+} wave in response to mechanical stimulation (cell 1). Scale bar, 50 μm. (**D**) The graph shows individual traces of self-ratios of fluo-4 fluorescence in keratinocytes (K1–K3) and DRG neuron (N4) shown in image **a** in **C**. Keratinocyte 1 was mechanically stimulated twice (arrows S1 and S2) separated by 5 min. The first and second mechanical stimulations were performed in the absence and presence of 100 units/ml apyrase (grey horizontal bar).

receptors results in phosphorylation of CREB (cAMP-response-element-binding protein) [45]. We showed that approx. 70% of both small-sized DRG neurons and NHEKs possess functional $P2Y_2$ receptors in the co-culture (Figure 5). In the peripheral skin-to-sensory neuron system, $P2Y_2$ receptors might be the main sensor for both NHEKs and DRG neurons. However, we cannot exclude the possibility that Ca^{2+} entry via P2X receptors is also involved in Ca^{2+} signalling in DRG neurons. In fact, when skin cells are killed, a large amount of intracellular ATP in the skin leaks and excites nociceptors by activating P2X receptors [46]. In a skin–nerve preparation, carrageenan inflammation of skin resulted in an increase in the activities of c-fibres, which was mediated by P2X receptors [47]. There might be multiple mechanisms by which the skin communicates with sensory neurons through ATP.

Apart from those of cell injury, the mechanisms underlying ATP release from NHEKs remain unknown. In neuronal cells, depolarizing stimulation resulted in exocytotic release of ATP in hippocampal slices [48] and cultured hippocampal neurons [49]. However, in non-excitable cells including NHEKs, the mechanism of ATP release is still a matter of debate. In astrocytes, there have been several reports that ATP can be released via chloride channels [50], gap junction hemi-channels [51], ATP-binding cassette [52] and exocytosis [53,54]. NHEKs also express several types of chloride channels [34,55,56], connexins [57–59] and SNARE (soluble *N*-ethylmaleimide-sensitive fusion protein attachment protein receptor) proteins [60,61]. Although these similarities raise the possibility that NHEKs and astrocytes might share the same mechanism for the release of ATP, further investigation is needed.

In summary, we demonstrated that extracellular ATP derived from NHEKs functions in both an autocrine and paracrine manner in the peripheral skin-to-sensory neurons system. Metabotropic $P2Y_2$ receptors may be important sensors for extracellular ATP in both NHEKs and small-sized DRG neurons.

We thank T. Obama (Division of Biosignaling, National Institute of Health Sciences) for helping in the culturing of cells and Y. Ohno (Division of Pharmacology, National Institute of Health Sciences) for continuous encouragement. This work was partially supported by the Organization for Pharmaceutical Safety and Research (Medical Frontier Project; MF-16), the Health Science Foundation (Japan) and Shiseido Research Center (Yokohama, Japan).

REFERENCES

1 Denda, M., Fuziwara, S., Inoue, K., Denda, S., Akamatsu, H., Tomitaka, A. and Matsunaga, K. (2001) Immunoreactivity of VR1 on epidermal keratinocyte of human skin. Biochem. Biophys. Res. Commun. **285**, 1250–1252
2 Inoue, K., Koizumi, S., Fuziwara, S., Denda, S. and Denda, M. (2002) Functional vanilloid receptors in cultured normal human epidermal keratinocytes. Biochem. Biophys. Res. Commun. **291**, 124–129
3 Grando, S. A. (1997) Biological functions of keratinocyte cholinergic receptors. J. Investig. Dermatol. Symp. Proc. **2**, 41–48
4 Arredondo, J., Nguyen, V. T., Chernyavsky, A. I., Bercovich, D., Orr-Urtreger, A., Kummer, W., Lips, K., Vetter, D. E. and Grando, S. A. (2002) Central role of α7 nicotinic receptor in differentiation of the stratified squamous epithelium. J. Cell Biol. **159**, 325–336
5 Genever, P. G., Maxfield, S. J., Kennovin, G. D., Mallman, J., Bowgen, C. J., Raxworthy, M. J. and Skerry, T. M. (1999) Evidence for a novel glutamate-mediated signaling pathway in keratinocytes. J. Invest. Dermatol. **112**, 337–342
6 Dixon, C. J., Bowler, W. B., Littlewood-Evans, A., Dillon, J. P., Bilbe, G., Sharpe, G. R. and Gallagher, J. A. (1999) Regulation of epidermal homeostasis through P2Y2 receptors. Br. J. Pharmacol. **127**, 1680–1686
7 Stoebner, P. E., Carayon, P., Penarier, G., Frechin, N., Barneon, G., Casellas, P., Cano, J. P., Meynadier, J. and Meunier, L. (1999) The expression of peripheral benzodiazepine receptors in human skin: the relationship with epidermal cell differentiation. Br. J. Dermatol. **140**, 1010–1016
8 Zia, S., Ndoye, A., Lee, T. X., Webber, R. J. and Grando, S. A. (2000) Receptor-mediated inhibition of keratinocyte migration by nicotine involves modulations of calcium influx and intracellular concentration. J. Pharmacol. Exp. Ther. **293**, 973–981
9 Watt, F. M., Hudson, D. L., Lamb, A. G., Bolsover, S. R., Silver, R. A., Aitchison, M. J. and Whitaker, M. (1991) Mitogens induce calcium transients in both dividing and terminally differentiating keratinocytes. J. Cell Sci. **99**, 397–405
10 Cornell-Bell, A. H., Finkbeiner, S. M., Cooper, M. S. and Smith, S. J. (1990) Glutamate induces calcium waves in cultured astrocytes: long-range glial signaling. Science **247**, 470–473
11 Charles, A. C., Merrill, J. E., Dirksen, E. R. and Sanderson, M. J. (1991) Intercellular signaling in glial cells: calcium waves and oscillations in response to mechanical stimulation and glutamate. Neuron **6**, 983–992
12 Thomas, A. P., Renard, D. C. and Rooney, T. A. (1991) Spatial and temporal organization of calcium signalling in hepatocytes. Cell Calcium **12**, 111–126
13 Hansen, M., Boitano, S., Dirksen, E. R. and Sanderson, M. J. (1993) Intercellular calcium signaling induced by extracellular adenosine 5′-triphosphate and mechanical stimulation in airway epithelial cells. J. Cell Sci. **106**, 995–1004
14 Demer, L. L., Wortham, C. M., Dirksen, E. R. and Sanderson, M. J. (1993) Mechanical stimulation induces intercellular calcium signaling in bovine aortic endothelial cells. Am. J. Physiol. **264**, H2094–H2102
15 Guthrie, P. B., Knappenberger, J., Segal, M., Bennett, M. V., Charles, A. C. and Kater, S. B. (1999) ATP released from astrocytes mediates glial calcium waves. J. Neurosci. **19**, 520–528
16 Scemes, E., Dermietzel, R. and Spray, D. C. (1998) Calcium waves between astrocytes from Cx43 knockout mice. Glia **24**, 65–73
17 Cauna, N. (1973) The free penicillate nerve endings of the human hairy skin. J. Anat. **115**, 277–288
18 Hilliges, M., Wang, L. and Johansson, O. (1995) Ultrastructural evidence for nerve fibers within all vital layers of the human epidermis. J. Invest. Dermatol. **104**, 134–137
19 Peier, A. M., Reeve, A. J., Andersson, D. A., Moqrich, A., Earley, T. J., Hergarden, A. C., Story, G. M., Colley, S., Hogenesch, J. B., McIntyre, P. et al. (2002) A heat-sensitive TRP channel expressed in keratinocytes. Science **296**, 2046–2049
20 Hensel, H. and Iggo, A. (1971) Analysis of cutaneous warm and cold fibres in primates. Pflugers Arch. **329**, 1–8
21 Hensel, H. and Kenshalo, D. R. (1969) Warm receptors in the nasal region of cats. J. Physiol. (Cambridge, U.K.) **204**, 99–112
22 Grynkiewicz, G., Poenie, M. and Tsien, R. Y. (1985) A new generation of Ca^{2+} indicators with greatly improved fluorescence properties. J. Biol. Chem. **260**, 3440–3450
23 Koizumi, S., Rosa, P., Willars, G. B., Challiss, R. A., Taverna, E., Francolini, M., Bootman, M. D., Lipp, P., Inoue, K., Roder, J. et al. (2002) Mechanisms underlying the neuronal calcium sensor-1-evoked enhancement of exocytosis in PC12 cells. J. Biol. Chem. **277**, 30315–30324
24 Koizumi, S., Bootman, M. D., Bobanovic, L. K., Schell, M. J., Berridge, M. J. and Lipp, P. (1999) Characterization of elementary Ca^{2+} release signals in NGF-differentiated PC12 cells and hippocampal neurons. Neuron **22**, 125–137
25 Communi, D., Pirotton, S., Parmentier, M. and Boeynaems, J. M. (1995) Cloning and functional expression of a human uridine nucleotide receptor. J. Biol. Chem. **270**, 30849–30852
26 Chang, K., Hanaoka, K., Kumada, M. and Takuwa, Y. (1995) Molecular cloning and functional analysis of a novel P2 nucleotide receptor. J. Biol. Chem. **270**, 26152–26158
27 Communi, D., Parmentier, M. and Boeynaems, J. M. (1996) Cloning, functional expression and tissue distribution of the human P2Y6 receptor. Biochem. Biophys. Res. Commun. **222**, 303–308
28 Communi, D., Motte, S., Boeynaems, J. M. and Pirotton, S. (1996) Pharmacological characterization of the human P2Y4 receptor. Eur. J. Pharmacol. **317**, 383–389
29 Greig, A. V., Linge, C., Terenghi, G., McGrouther, D. A. and Burnstock, G. (2003) Purinergic receptors are part of functional signaling system for proliferation and differentiation of human epidermis keratinocytes. J. Invest. Dermatol. **120**, 1007–1015
30 Fam, S. R., Gallagher, C. J. and Salter, M. W. (2000) P2Y1 purinoceptor-mediated Ca^{2+} signaling and Ca^{2+} wave propagation in dorsal spinal cord astrocytes. J. Neurosci. **20**, 2800–2808
31 Newman, E. A. and Zahs, K. R. (1998) Modulation of neuronal activity by glial cells in the retina. J. Neurosci. **18**, 4022–4028
32 Finkbeiner, S. (1992) Calcium waves in astrocytes – filling in the gaps. Neuron **8**, 1101–1108
33 Burgstahler, R., Koegel, H., Rucker, F., Tracey, D., Grafe, P. and Alzheimer, C. (2003) Confocal ratiometric voltage imaging of cultured human keratinocytes reveals layer-specific responses to ATP. Am. J. Physiol. **284**, C944–C952
34 Koegel, H. and Alzheimer, C. (2001) Expression and biological significance of Ca^{2+}-activated ion channels in human keratinocytes. FASEB J. **15**, 145–154

35 Denda, M., Inoue, K., Fuziwara, S. and Denda, S. (2002) P2X purinergic receptor antagonist accelerates skin barrier repair and prevents epidermal hyperplasia induced by skin barrier disruption. J. Invest. Dermatol. **119**, 1034–1040
36 Koizumi, S., Fujishita, K., Tsuda, M., Shigemoto-Mogami, Y. and Inoue, K. (2003) Dynamic inhibition of excitatory synaptic transmission by astrocyte-derived ATP in hippocampal cultures. Proc. Natl. Acad. Sci. U.S.A. **100**, 11023–11028
37 Newman, E. A. (2003) Glial cell inhibition of neurons by release of ATP. J. Neurosci. **23**, 1659–1666
38 Tsuda, M., Shigemoto-Mogami, Y., Koizumi, S., Mizokoshi, A., Kohsaka, S., Salter, M. W. and Inoue, K. (2003) P2X4 receptors induced in spinal microglia gate tactile allodynia after nerve injury. Nature (London) **424**, 778–783
39 Cervero, F. (1994) Sensory innervation of the viscera: peripheral basis of visceral pain. Physiol. Rev. **74**, 95–138
40 Nakamura, F. and Strittmatter, S. M. (1996) P2Y1 purinergic receptors in sensory neurons: contribution to touch-induced impulse generation. Proc. Natl. Acad. Sci. U.S.A. **93**, 10465–10470
41 Burnstock, G. (2000) P2X receptors in sensory neurones. Br. J. Anaesth. **84**, 476–488
42 Tsuda, M., Koizumi, S., Kita, A., Shigemoto, Y., Ueno, S. and Inoue, K. (2000) Mechanical allodynia caused by intraplantar injection of P2X receptor agonist in rats: involvement of heteromeric P2X2/3 receptor signaling in capsaicin-insensitive primary afferent neurons. J. Neurosci. **20**, RC90
43 Tominaga, M., Wada, M. and Masu, M. (2001) Potentiation of capsaicin receptor activity by metabotropic ATP receptors as a possible mechanism for ATP-evoked pain and hyperalgesia. Proc. Natl. Acad. Sci. U.S.A. **98**, 6951–6956
44 Sanada, M., Yasuda, H., Omatsu-Kanbe, M., Sango, K., Isono, T., Matsuura, H. and Kikkawa, R. (2002) Increase in intracellular Ca^{2+} and calcitonin gene-related peptide release through metabotropic P2Y receptors in rat dorsal root ganglion neurons. Neuroscience **111**, 413–422
45 Molliver, D. C., Cook, S. P., Carlsten, J. A., Wright, D. E. and McCleskey, E. W. (2002) ATP and UTP excite sensory neurons and induce CREB phosphorylation through the metabotropic receptor, P2Y2. Eur. J. Neurosci. **16**, 1850–1860
46 Cook, S. P. and McCleskey, E. W. (2002) Cell damage excites nociceptors through release of cytosolic ATP. Pain **95**, 41–47
47 Hamilton, S. G., McMahon, S. B. and Lewin, G. R. (2001) Selective activation of nociceptors by P2X receptor agonists in normal and inflamed rat skin. J. Physiol. (Cambridge, U.K.) **534**, 437–445
48 Wieraszko, A., Goldsmith, G. and Seyfried, T. N. (1989) Stimulation-dependent release of adenosine triphosphate from hippocampal slices. Brain Res. **485**, 244–250
49 Koizumi, S., Fujishita, K., Tsuda, M. and Inoue, K. (2003) Neuron-to-astrocyte communication by endogenous ATP in mixed culture of rat hippocampal neurons and astrocyte. Drug Dev. Res. **59**, 88–94
50 Darby, M., Kuzmiski, J. B., Panenka, W., Feighan, D. and MacVicar, B. A. (2003) ATP released from astrocytes during swelling activates chloride channels. J. Neurophysiol. **89**, 1870–1877
51 Stout, C. E., Costantin, J. L., Naus, C. C. and Charles, A. C. (2002) Intercellular calcium signaling in astrocytes via ATP release through connexin hemichannels. J. Biol. Chem. **277**, 10482–10488
52 Ballerini, P., Di Iorio, P., Ciccarelli, R., Nargi, E., D'Alimonte, I., Traversa, U., Rathbone, M. P. and Caciagli, F. (2002) Glial cells express multiple ATP binding cassette proteins which are involved in ATP release. Neuroreport **13**, 1789–1792
53 Malenschein, V., Marxen, M., Volknandt, W. and Zimmermann, H. (1999) A plethora of presynaptic proteins associated with ATP-storing organelles in cultured astrocytes. Glia **26**, 233–244
54 Coco, S., Calegari, F., Pravettoni, E., Pozzi, D., Taverna, E., Rosa, P., Matteoli, M. and Verderio, C. (2003) Storage and release of ATP from astrocytes in culture. J. Biol. Chem. **278**, 1354–1362
55 Galietta, L. J., Barone, V., de Luca, M. and Romeo, G. (1991) Characterization of chloride and cation channels in cultured human keratinocytes. Pflugers Arch. **418**, 18–25
56 Mastrocola, T., de Luca, M. and Rugolo, M. (1991) Characterization of chloride transport pathways in cultured human keratinocytes. Biochim. Biophys. Acta **1097**, 275–282
57 Risek, B. and Gilula, N. B. (1991) Spatiotemporal expression of three gap junction gene products involved in fetomaternal communication during rat pregnancy. Development **113**, 165–181
58 Di, W. L., Rugg, E. L., Leigh, I. M. and Kelsell, D. P. (2001) Multiple epidermal connexins are expressed in different keratinocyte subpopulations including connexin 31. J. Invest. Dermatol. **117**, 958–964
59 Plum, A., Hallas, G. and Willecke, K. (2002) Expression of the mouse gap junction gene Gjb3 is regulated by distinct mechanisms in embryonic stem cells and keratinocytes. Genomics **79**, 24–30
60 Scott, G. and Zhao, Q. (2001) Rab3a and SNARE proteins: potential regulators of melanosome movement. J. Invest. Dermatol. **116**, 296–304
61 Scott, G., Leopardi, S., Printup, S. and Madden, B. C. (2002) Filopodia are conduits for melanosome transfer to keratinocytes. J. Cell Sci. **115**, 1441–1451

Received 21 July 2003/23 December 2003; accepted 16 February 2004
Published as BJ Immediate Publication 16 February 2004, DOI 10.1042/BJ20031089

GLIA 49:288–300 (2005)

Cytoprotection Against Oxidative Stress-Induced Damage of Astrocytes by Extracellular ATP Via $P2Y_1$ Receptors

YOUICHI SHINOZAKI,[1,4] SCHUICHI KOIZUMI,[2] SEIICHI ISHIDA,[2] JUN-ICHI SAWADA,[3] YASUO OHNO,[2] AND KAZUHIDE INOUE[1,4]*

[1]*Division of Biosignaling, National Institute of Health Sciences, Setagaya, Tokyo, Japan*
[2]*Division of Pharmacology, National Institute of Health Sciences, Setagaya, Tokyo, Japan*
[3]*Division of Biochemistry and Immunochemistry, National Institute of Health Sciences, Setagaya, Tokyo, Japan*
[4]*Department of Molecular and System Pharmacology, Graduate School of Pharmaceutical Sciences, Kyushu University, Fukuoka, Japan*

KEY WORDS ATP; $P2Y_1$ receptors; astrocytes; oxidative stress

ABSTRACT Oxidative stress is the main cause of neuronal damage in traumatic brain injury, hypoxia/reperfusion injury, and neurodegenerative disorders. Although extracellular nucleosides, especially adenosine, are well known to protect against neuronal damage in such pathological conditions, the effects of these nucleosides or nucleotides on glial cell damage remain largely unknown. We report that ATP but not adenosine protects against the cell death of cultured astrocytes induced by hydrogen peroxide (H_2O_2). ATP ameliorated the H_2O_2-induced decrease in cell viability of astrocytes in an incubation time- and concentration-dependent fashion. Protection by ATP was inhibited by P2 receptor antagonists and was mimicked by $P2Y_1$ receptor agonists but not by adenosine. The expressions of $P2Y_1$ mRNAs and functional $P2Y_1$ receptors in astrocytes were confirmed. Thus, ATP, acting on $P2Y_1$ receptors in astrocytes, showed a protective action against H_2O_2. The astrocytic protection by the $P2Y_1$ receptor agonist 2-methylthio-ADP was inhibited by an intracellular Ca^{2+} chelator and a blocker of phospholipase C, indicating the involvement of intracellular signals mediated by Gq/11-coupled $P2Y_1$ receptors. The ATP-induced protection was inhibited by cycloheximide, a protein synthesis inhibitor, and it took more than 12 h for the onset of the protective action. In the DNA microarray analysis, ATP induced a dramatic upregulation of various oxidoreductase genes. Taken together, ATP acts on $P2Y_1$ receptors coupled to Gq/11, resulting in the upregulation of oxidoreductase genes, leading to the protection of astrocytes against H_2O_2.

INTRODUCTION

Astrocytes are much more than merely support cells for neurons in the central nervous system (CNS). They can receive inputs, assimilate information, and send instructive chemical signals to neighboring glial cells as well as neurons (Araque et al., 1999a, b, 2001; Haydon, 2001). Thus, communication among astrocytes would play an important role in brain function. Initially, so-called gliotransmission, a glia-to-glia communication or even neuron-to-glia communication, was reported to be mediated by glutamate (Cornell-Bell et al., 1990; Charles et al., 1991; Parpura et al., 1994; Innocenti et al., 2000) because astrocytes express glutamate receptors and release glutamate. However, re-

Grant sponsor: Program for Promotion of Fundamental Studies in Health Sciences of the Organization for Pharmaceutical Safety and Research (OPSR); Grant number: MF-16; Grant number: MPJ-6; Grant sponsor: Grant-in-Aid for Scientific Research; Grant sponsor: Brain Science Foundation.

*Correspondence to: Kazuhide Inoue, Division of Biosignaling, National Institute of Health Sciences, 1-18-1 Kamiyoga, Setagaya, Tokyo 158-8501, Japan. E-mail: inoue@nihs.go.jp

Received 29 March 2004; Accepted 30 July 2004

DOI 10.1002/glia.20118

Published online 19 October 2004 in Wiley InterScience (www.interscience.wiley.com).

cent accumulating evidence has shown that extracellular ATP released from astrocytes has a central role in astrocyte-to-astrocyte (Guthrie et al., 1999), astrocyte-to-microglia (Verderio and Matteoli, 2001; Schipke et al., 2002), and even astrocyte-to-neuron communication (Koizumi et al., 2003; Newman, 2003; Zhang et al., 2003).

ATP is an endogenous ligand for P2 receptors that are classified into ligand-gated P2X and G-protein-coupled metabotropic P2Y receptors (Abbracchio and Burnstock, 1994). Astrocytes express both types of P2 receptors (James and Butt, 2002; Fumagalli et al., 2003) and can release ATP in response to various stimuli (Guthrie et al., 1999; Queiroz et al., 1999; Koizumi et al., 2003). Astrocytic ATP acting on these P2 receptors forms intercellular Ca^{2+} waves that mediate long-range communications in astrocytes (Fam et al., 2000; Gallagher and Salter, 2003). However, the physiological or pathological significance of such an ATP/P2 receptor-mediated response in astrocytes remains largely unknown.

It has been reported that ATP inhibits excess neuronal excitations by inhibiting the release of glutamate (Koizumi and Inoue, 1997; Zhang et al., 2003) or by facilitating inhibitory γ-aminobutyric acid (GABA) release in the hippocampus (Aihara et al., 2002) and is therefore presumably involved in protecting neurons against excitotoxicity. With regard to neuroprotective actions, however, adenosine, a metabolite of ATP, has received much attention as an important inhibitory molecule because it is formed by the immediate degradation of ATP by ectonucleotidases, potently inhibiting the excitability of neurons and protecting them against various neurodegenerative disorders including excitatory neuronal death (Jones et al., 1998; Behan and Stone, 2002; Hentschel et al., 2003; Schwarzschild et al., 2003). This might be why the functional role of ATP in relation to neuroprotection has received only limited attention. Interestingly, however, adenosine does not show any protective action in astrocytes, rather it induces the cell death of astrocytes (Abbracchio et al., 1995; Appel et al., 2001; Di Iorio et al., 2002). It has been reported that ATP protects astrocytes against glucose deprivation-induced cell death, although this protection appears to be independent of P2 receptors (Shin et al., 2002). ATP is released from both neurons (Wieraszko et al., 1989; Inoue et al., 1995) and astrocytes (Guthrie et al., 1999; Ahmed et al., 2000) in physiological and pathological conditions, and astrocytes could receive the ATP signal via various P2 receptors, including a high-affinity $P2Y_1$ receptor (Koizumi et al., 2002). These findings raise the possibility that, unlike neurons, astrocytes mainly use ATP/P2 receptor-mediated pathway(s) for their own survival.

We report that ATP acting on $P2Y_1$ receptors protects astrocytes from cell death induced by hydrogen peroxide (H_2O_2), one of the main reactive oxygen species (ROS) generated by traumatic brain injury, hypoxia/reperfusion, and various neurodegenerative disorders (Agardh et al., 1991; Lei et al., 1997; Cuajungco et al., 2000; Huang et al., 2000; Tabner et al., 2001; Tamagno et al., 2003). We further demonstrate by using differential gene expression analysis that ATP induces the upregulation of oxidoreductase genes, suggesting the involvement of these genes in the protective action.

MATERIALS AND METHODS

Chemicals

Adenosine 5′-triphosphate (ATP), adenosine 5′-diphosphate (ADP), uridine 5′-triphosphate (UTP), adenosine, 2-methylthio-adenosine diphosphate (2MeSADP), adenosine 5-o-(2-thiodiphophate) (ADPβS), α,β-methylene-adenosine triphosphate (α,βmeATP), suramin, reactive blue 2 (RB2), pyridoxal-phosphate-6-azophenyl-2′,4′-disulfonic acid (PPADS), MRS2179, U73122, U73343, glutamate, 1-octanol, DL-2-amino-5-phosphonopentanoic acid (AP-V), 6-cyano-7-nitroquinoxaline-2,3-dione (CNQX) and (RS)-α-methyl-4-carboxyphenylglycine (MCPG) were purchased from Sigma Chemical Co. (St Louis, MO). The sources of other chemicals are shown in parentheses as follows; trypsin-EDTA, M-MLV reverse transcriptase, 100 mM dNTP set, recombinant ribonuclease (RNase) inhibitor and deoxyribonuclease (DNase) I (GIBCO/Invitrogen, Tokyo, Japan), RNA STAT 60 (Tel-Test, Friendswood, TX), hydrogen peroxide (H_2O_2) (Wako Pure Chemicals, Osaka, Japan), 3-(4,5-dimethylthiazol-2-y1)-2,5-diphenyltetrazolium bromide (MTT) assay kit (Chemicon International, Temecula, CA), GeneAmp PCR Reagent Kit and AmpliTaq DNA polymerase (Perkin-Elmer, (Foster City, CA) Roche Molecular Systems, (Pleasanton, CA), O,O′-Bis (2-aminophenyl) ethyleneglycol-N,N,N′,N′-tetraacetic acid, tetraacetoxymethyl ester (BAPTA-AM) (Calbiochem Biosciences, San Diego, CA).

Cells and Cell Culture

Astrocytes were prepared from neonatal rat forebrain. The cells were cultured in Dulbecco's modified essential medium (DMEM, GIBCO/Invitrogen) supplemented with 10% fetal bovine serum (FBS; GIBCO/Invitrogen). After 3 weeks with changing of the medium every 3 days, the medium was changed to DMEM with 5% horse serum (HS; GIBCO/Invitrogen) and 5% FBS; the cells were shaken for 15 h at 100 rpm. Then, the cells were washed 3 times with phosphate-buffered saline (PBS) (10 ml each) and supplemented with 0.025% trypsine-EDTA (diluted with PBS), and incubated for 2 min under 10% CO_2 /90% air at 37°C. After the cells were harvested, 2×10^5 cells were seeded on 60 × 15-mm dishes (Falcon/Becton Dickinson, San Jose, CA) and cultured in DMEM with 5% HS and 5% FBS. Total RNA was collected from five dishes. For the cell viability assay, cells were seeded on 96-well plates (NUNC, Roskilde, Denmark) at a density of 1.25×10^4 cells/well. At 24 h after the seeding, the medium was

changed. The cells were used for experiments 72 h after the medium exchange.

Experimental Design of Hydrogen Peroxide (H_2O_2)-Evoked Cell Death

Astrocytes were exposed to various concentrations of H_2O_2 (75–300 μM) for 1–24 h, and then the cell viability was investigated. In the present study, we chose a H_2O_2 concentration of 250 μM and an incubation period of 2 h to assess the effect of ATP.

Cell Viability Assay

For the cell viability assay, we used an MTT assay. MTT is a yellow tetrazolium salt that is reduced to purple formazan (Altman, 1976). The MTT assay assesses cell viability by measuring the mitochondrial function (Twentyman and Luscombe, 1987). After incubation with H_2O_2 for 2 h, a 1/10 volume of MTT solution (5 mg/ml in PBS) was added and incubated for 4 h under 10% CO_2/90% air at 37°C. Then an equal volume of isopropanol (with 0.04 N HCl) was added to the cells, and the MTT formazan was dissolved by pipetting. The absorbance was measured on an enzyme-linked immunosorbent assay (ELISA) plate reader (ASYS Hitech, Eugendorf, Austria) with a test and reference wavelength of 570 and 630 nm, respectively.

Expression of $P2Y_1$ Receptors in Astrocytes

The expression of $P2Y_1$ receptor mRNA was analyzed by single reverse transcription-polymerase chain reaction (RT-PCR). For RT-PCR analysis, astrocytes were directly lysed with 0.5 ml of RNA STAT-60 (Tel-Test B) and total RNA was isolated; 1 μg of RNA was reverse-transcribed with M-MLV transcriptase. Aliquots (1 μl) of the RT product were added to the reaction mixture containing 1 × PCR buffer (10 mM Tris-HCl, pH 8.3, 50 mM KCl), 1.5 mM $MgCl_2$, 0.2 mM dNTPs, 2.5 U of *Taq* polymerase and $P2Y_1$ receptors specific primers according to the nucleotide sequences as follows; forward, 5′-ctgatcttgggctgttatgg-3′ and reverse, 5′-gctgttgagacttgctagac-3′. Amplification was performed in a Gene Amp PCR System 2400-R (Perkin-Elmer/Roche Molecular Systems) thermal cycler for 30–40 cycles, after an initial denaturation at 94°C for 2 min by utilizing sense and antisense primers specifically designed for $P2Y_1$ receptors. The PCR product was resolved on agarose gel stained by 2% ethidium bromide and visualized under ultraviolet (UV) light.

Measurement of Intracellular Ca^{2+} Concentration ($[Ca^{2+}]_i$) in Single Cells

The increase in $[Ca^{2+}]_i$ in single cells was measured by the fura-2 method as described by Grynkiewicz et al. (1985) with minor modifications (Koizumi et al., 2002). In brief, the cells were washed with a balanced salt solution (BSS) of the following composition (in mM): NaCl 150, KCl 5.0, $CaCl_2$ 1.8, $MgCl_2$ 1.2, N-2-hydroxyethylpiperazine-N′-2-ethanesulfonic acid (HEPES) 25, and D-glucose 10 (pH = 7.4). Cells were then loaded with 5 μM fura-2 acetoxymethylester (fura-2 AM) at room temperature in BSS for 45 min, followed by a BSS wash and a further 30-min incubation to allow deesterification of the loaded dye. For the Ca^{2+}-free experiment, Ca^{2+} was removed from the BSS (Ca^{2+}-free BSS). The coverslips were mounted on an inverted epifluorescence microscope (TE-2000-U, Nikon, Tokyo, Japan). Fluorescent images were obtained by alternate excitation at 340 nm (F340) and 380 nm (F380). The emission signal at 510 nm was collected by a charge-coupled device camera (C-6790, Hamamatsu Photonics, Hamamatsu, Japan) coupled with an image intensifier (GaAsP, C8600-03, Hamamatsu Photonics); digitized signals were stored and processed using an image processing system (Aquacosmos, Hamamatsu Photonics). Drugs were dissolved in BSS and applied by superfusion.

Measurement of Extracellular ATP Concentration

The extracellular ATP concentration in astrocytes was detected with a luciferin-luciferase bioluminescence assay. After glutamate stimulation or exogenous ATP application, supernatants were collected at different time points and were mixed with luciferase reagents (ATP bioluminescence assay kit CLS II; Roche Diagnostics, Mannheim, Germany). ATP bioluminescence was detected by a luminometer (Lumiphotometer TD-4000, Labo Science, Tokyo, Japan). The absolute ATP concentration was estimated using a standard ATP solution (0.001–1 μM).

Total RNA Preparation

After washing the cells twice with PBS, total RNA was prepared with RNeasy Mini total RNA Preparation Kit (Qiagen GmbH, Tokyo, Japan) according to the manufacturer's instructions.

DNA Microarray Analysis

Converting total RNA to the targets for Affymetrix GeneChip DNA microarray hybridization was done according to the manufacturer's instructions. The targets were hybridized to rat genome U34A Gene Chip microarray (Affymetrix) for 16–24 h at 45°C. After the hybridization, the DNA microarrays were washed and stained on Fluidics Station (Affymetrix) according to the protocol provided by Affymetrix. Then, the DNA microarrays were scanned, and the images obtained

were analyzed by Microarray Suite Expression Analysis Software (version 5.0; Affymetrix). To analyze the gene expressions in astrocytes, differences in the mean level of the gene expression index between the control group and drug-treated group were assessed using the Student's *t*-test for each probeset.

Astrocytes were incubated for 2 h with ATP at a final concentration of 100 μM. Total RNA was prepared at the end of incubation and converted to the target for GeneChip hybridization. The gene expression was analyzed in duplicate by Rat Genome U34A GeneChip using these targets. The addition of ATP and the preparation of total RNA was done four times independently.

Selection of Differentially Expressed Genes

The first step was selecting genes whose expression levels were increased 2-fold by treatment with ATP. The second step was selecting genes whose *P*-values were $P < 0.05$ using Student's *t*-test. The last step was selecting genes whose expression levels of the drug treated group were 1,000.

Quantitative RT-PCR of Oxidoreductase Genes

RT-PCR amplifications were performed using Taqman One-step RT-PCR Master Mix Reagents and, 200 nM oxidoreductase-specific primers. Using the computer software Primer Express (Applied Biosystems), clone-specific primers were designed to recognize rat oxidoreductase genes, i.e., rat carbonyl reductase (CBR, Taqman Probe, 5′-cctcctgaatgcctgccctg-3′; forward, 5′-tgaggagaggagagaggacaaga-3′; reverse, 5′-cctgccatgtcggttctga-3′), schlafen-4 (SHL4, Taqman probe, 5′-aggccttatcgaggccagatggtttg-3′; forward, 5′-tcttgtttcctagaactgttgtg-3′; reverse, 5′-ggtgaggtagcctggctatagc-3′), and thioredoxin reductase (TrxR, Taqman probe, 5′-attgaagcagggacaccaggccg-3′; forward, 5′-gtgccgacgaaaattgaaca-3′; reverse, 5′-gtggatttagcggtcacctga-3′). RT-PCR was performed by 30 min reverse transcription at 48°C, 10 min Amplitaq Gold activation at 95°C, then 15-s denaturation at 95°C, 1 min annealing and elongation at 60°C for 40 cycles in a PRISM7700 (Applied Biosystems). To exclude contamination by nonspecific PCR products such as primer dimmers, melting curve analysis was applied to all final PCR protocols after the cycling protocol. Each experiment was performed in triplicate.

RESULTS

Protection by ATP Against Oxidative Stress-Induced Cell Death in Astrocytes

Using an MTT assay, we tested the effect of hydrogen peroxide (H_2O_2) on cell viability in astrocytes. We found that H_2O_2 caused a time- (Fig. 1A) and concentration-dependent (Fig. 1B) decrease in the cell viability of the astrocytes, i.e., cell death of the astrocytes. When incubated for 1 h at 250 μM, the cell viability was almost halved and then was gradually decreased to ~20% of the non-treated control level by a further incubation (2–24 h, Fig. 1A). When the H_2O_2 concentrations were varied, the cell viability was decreased in a concentration-dependent fashion and reached the minimum at 250 μM. We therefore chose an H_2O_2 concentration of 250 μM and an incubation period of 2 h for the following experiments.

We tested the effect of exogenously applied ATP on the H_2O_2-induced astrocytic cell death. ATP was applied to the cells 24 h before and during H_2O_2 applica-

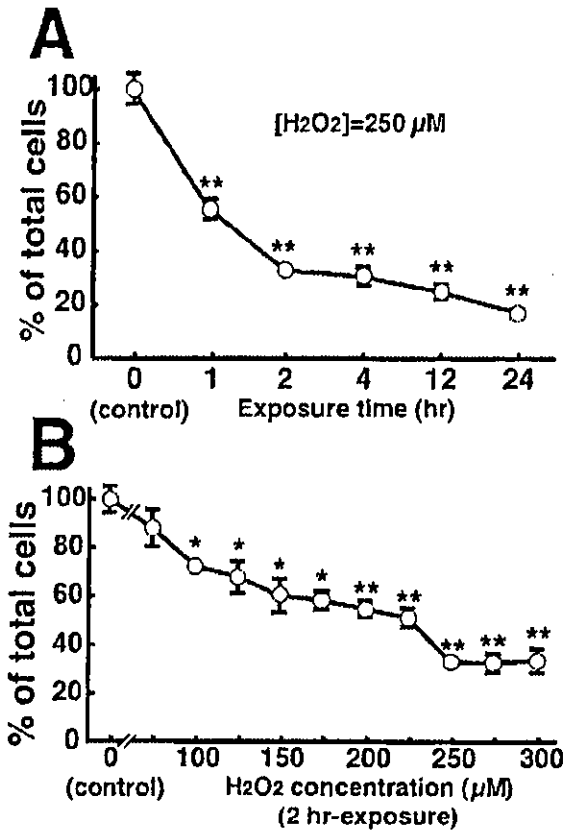

Fig. 1. Changes in cell viability of astrocytes by H_2O_2. A: Cells were incubated with 250 μM H_2O_2 for various periods before the cell viability test. The cell viability was evaluated by the MTT assay as described in Materials and Methods. H_2O_2 induced a decrease in cell viability in an exposure time-dependent fashion. B: Cells were stimulated with various concentrations of H_2O_2 for 2 h; cell viability was then examined. H_2O_2 evoked cell death in a concentration-dependent fashion. Sequential plots show mean ± SEM of triplicate measurements, depicting a representative experiment (n = 3). Values were normalized to total cell number (control) and the cell viability was expressed as percentage of total cell. Asterisks show significant differences from the control response ($^*P < 0.05$, $^{**}P < 0.01$, Student's *t*-test).

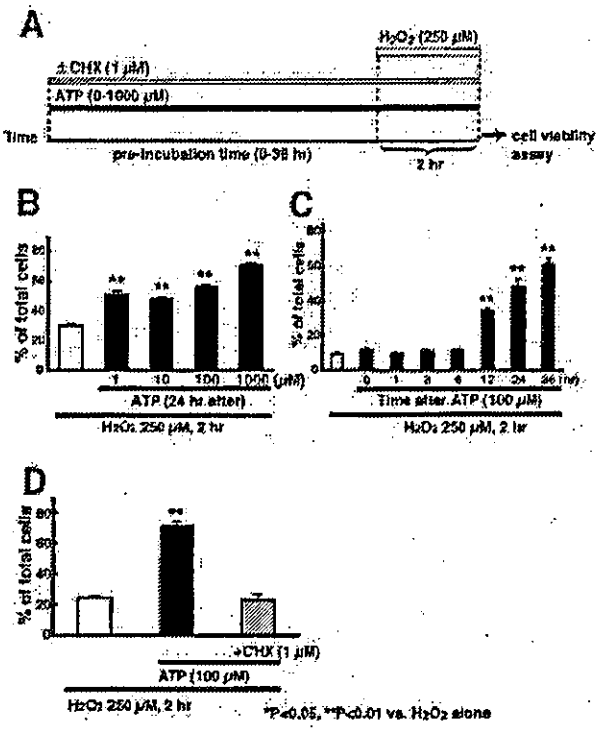

Fig. 2. Protection by ATP of H_2O_2-evoked cell death in astrocytes. A: Stimulus regime. B: ATP protected against H_2O_2-evoked cell death in a concentration-dependent fashion. Cells were incubated with ATP (1–1,000 μM) 24 h before and during H_2O_2 application. C: Protective effect of ATP was dependent on the duration of preincubation. Cells were incubated with ATP (100 μM) for various periods (from 0 to 36 h), and then exposed to H_2O_2 together with ATP. Without any preincubation periods, ATP did not show any significant protective effect. D: Inhibition by CHX of the ATP-induced protection. Incubation of cells with CHX (1 μM for 24 h) abolished the protective effect of ATP. Each histogram shows a typical experiment with each data point being mean ± SEM of triplicate measurements. At least three such experiments were performed. Values were normalized to total cell number and the cell viability was expressed as percentage of total cell number. Asterisks show significant difference from the response evoked by H_2O_2 alone (*$P < 0.05$, **$P < 0.01$, Student's t-test).

tion. Pretreatment with ATP significantly inhibited the H_2O_2-induced cell death in a concentration-dependent manner over a concentration range of 1–1,000 μM (Fig. 2B). When pretreated for 12–36 h, the H_2O_2-induced cell death in astrocytes was significantly reduced to about 60% of control (Fig. 2C). However, ATP did not show any cytoprotective action when the exposure time of ATP was less than 12 h. When astrocytes were pretreated with ATP plus cycloheximide (CHX, 1 μM), a protein synthesis inhibitor, the protection by ATP (100 μM for 24 h) disappeared (Fig. 2D). CHX alone had no effect on the viability of astrocytes (control; 100 ± 6%, CHX 1 μM; 90 ± 6%, n = 6).

Protection by ATP against the H_2O_2-induced cell death of astrocytes was evaluated pharmacologically. As shown in Figure 3B, when the P2 receptor antagonists suramin (100 μM), PPADS (300 μM), and RB2 (10 μM) were added to the cells 15 min before and during ATP (100 μM) application, ATP protection was almost abolished, indicating the involvement of P2 receptors. UTP (100 and 1,000 μM), an agonist of $P2Y_2$ and $P2Y_4$ receptors, α,βmeATP (100 μM), an agonist of $P2X_1$ and $P2X_3$ receptors, had no effect on the H_2O_2-evoked cell death (Fig. 3C). Adenosine (10 μM) did not show any protection against the cell death. The $P2Y_1$ receptor agonists 2MeSADP (1 μM) and ADPβS (1 μM) provided significant protection against cell death (Fig. 3D) and the ATP-induced protection was inhibited by the $P2Y_1$ receptor antagonist MRS2179 in a concentration-dependent manner (Fig. 3E). Thus, ATP appears to show its protective action mainly via a $P2Y_1$ receptor-mediated pathway(s) in astrocytes. None of the agonists and antagonists alone had any effect on the cell viability of astrocytes (Fig. 3B–E, gray columns).

We tested whether prolonged ATP is required or a brief exposure of ATP is enough to trigger its protective action in astrocytes. Since the ATP-induced protection is mediated by $P2Y_1$ receptors (Fig. 3), we added the $P2Y_1$ receptor antagonist MRS2179 (1 μM) to the culture medium 15 min before or 30 min after ATP stimulation, and then further incubated for 24 h prior to H_2O_2 exposure. MRS2179 reversed the ATP-induced protection only when it was added to the cells 15 min before and during ATP stimulation (MRS2179 15 min before ATP, 33.6 ± 5.9% of total cells, n = 3, $P = 0.91$ vs. H_2O_2 alone; MRS2179 30 min after ATP, 62.9 ± 3.5 of total cells, n = 3, $P < 0.05$ vs. H_2O_2 alone; Fig. 4B). Furthermore, we analyzed the time-course of ATP degradation in astrocytes. ATP was exogenously applied to astrocytes, and the supernatants were collected at different incubation periods. Exogenously applied ATP (100 μM) was soon metabolized; the concentrations at 5, 15, 30, 60, and 120 min were 76.0 ± 17.8, 18.9 ± 23.7, 1.2 ± 1.0, 0.3 ± 0.36 and 0.02 ± 0.03 μM, respectively (Fig. 4C). Although longer periods (>12 h, see Fig. 2C) were required for the onset of the cytoprotective action, prolonged exposure of ATP was not necessarily required for the protection in astrocytes.

Intracellular Signaling Cascades Involved in $P2Y_1$ Receptor-Mediated Protection

We investigated the involvement of $P2Y_1$ receptor-mediated intracellular signaling cascades in the protection against the H_2O_2-induced cell death in astrocytes. Both the PLC inhibitor U73122 (5 μM) and the rapid intracellular Ca^{2+} chelator BAPTA-AM (25 μM) inhibited the protection by 1 μM 2MeSADP (Fig. 5). The much less active PLC inhibitor U73343 (5 μM) had no effect on the ATP-evoked protection. These chemicals were added to the cells 1 h before and during 2MeSADP-application and were washed away before H_2O_2 application. These blockers themselves had no effect on the cell viability under the normal condition (control, 100 ± 3%; U73122, 90 ± 5%; U73343, 92 ± 6%; and BAPTA-AM, 105 ± 3%, n = 6) (Fig. 5B, gray columns) nor affected the H_2O_2-induced cell death in

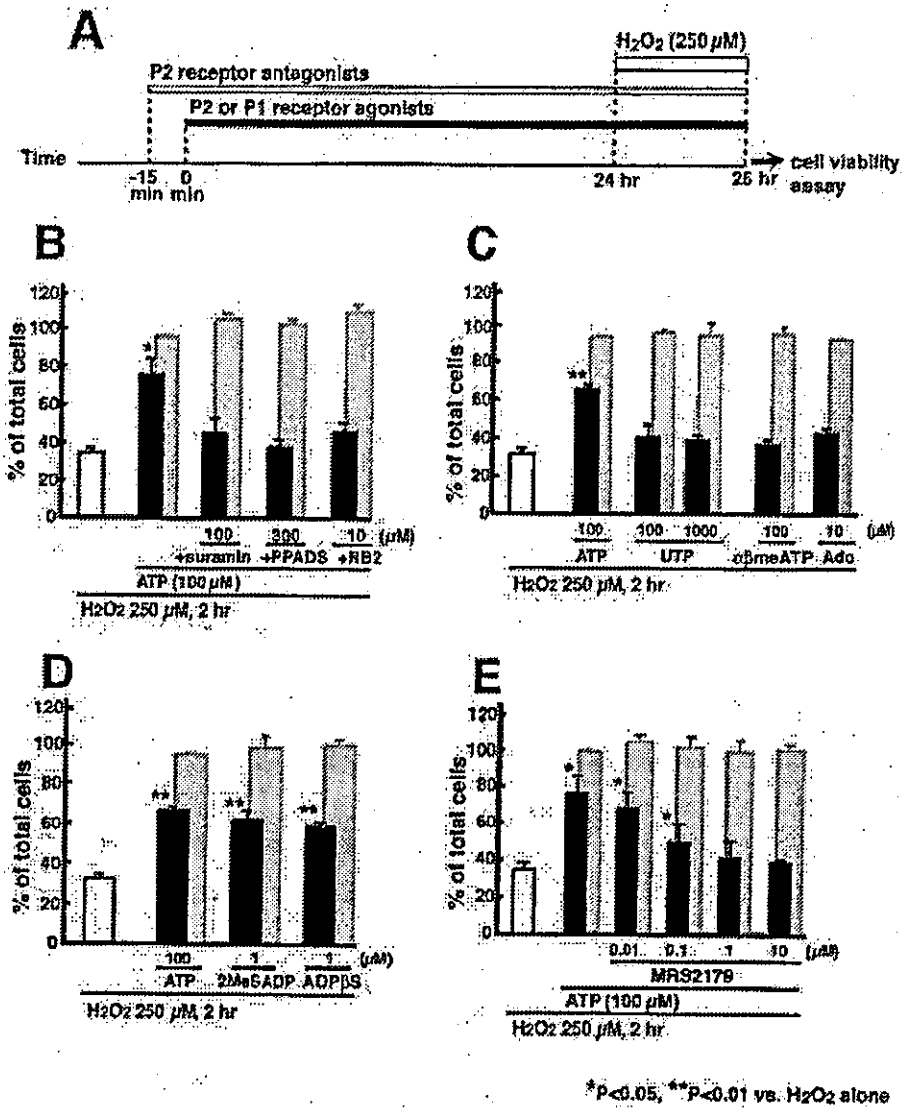

Fig. 3. Effect of P2 receptor agonists and antagonists on the H_2O_2-evoked cell death of astrocytes. A: Stimulus regime. B: Inhibition by P2 receptor antagonists of ATP-induced protection. Suramin (100 μM), PPADS (300 μM) and RB2 (10 μM) reversed the effect of ATP. Cells were incubated with ATP (100 μM) for 24 h before H_2O_2 application. Each antagonist was added to the cells 15 min before and during ATP application. C: Effect of P1 and P2 receptor agonists. UTP (100 and 1,000 μM), α,βmeATP (100 μM) and adenosine (Ado, 10 μM) had no significant protective effect against the H_2O_2-evoked death in astrocytes. D: Protection by $P2Y_1$ selective agonists of H_2O_2-evoked cell death in astrocytes. The $P2Y_1$ selective agonists 2MeSADP and ADPβS (1 μM) mimicked the cytoprotective effect of ATP. E: Inhibition by $P2Y_1$ selective antagonist of ATP-induced protection. The $P2Y_1$ selective antagonist MRS2179 inhibited the effect of ATP in a concentration-dependent manner. Various concentrations of MRS2179 were added to the cells 15 min before and during ATP application. Gray columns show the effects of agonists or antagonists alone on the cell viability in the normal condition. Each histogram shows a typical experiment with each data point being mean ± SEM of triplicate measurements. At least three such experiments were performed. Values were normalized to total cell number. Asterisks show significant difference from the response evoked by H_2O_2 alone (*$P < 0.05$. **$P < 0.01$, Student's t-test).

astrocytes (H_2O_2 alone, 36 ± 2%; +U73122, 36 ± 1%; +U73343, 34 ± 4%; and BAPTA-AM, 35 ± 13%, n = 6).

We also studied the effect of these blockers on the 2MeSADP-evoked increase in $[Ca^{2+}]_i$ in astrocytes (Fig. 5C). Both BAPTA-AM (25 μM) and U73122 (5 μM) inhibited the 2MeSADP-evoked increase in $[Ca^{2+}]_i$, whereas U73343 (5 μM) did not. BAPTA-AM and U73122 also reduced 2MeSADP-responders (Fig. 5C, open circles). U73122, U73343 and BAPTA-AM were added to the cells 15 min before and during 2MeSADP application.

Glutamate is another important gliotransmitter that leads to an increase in $[Ca^{2+}]_i$ in astrocytes via PLC-linked metabotropic glutamate receptors (Pasti et al., 1997; Porter and McCarthy, 1996). We therefore tested the effect of pretreatment with glutamate on the H_2O_2-induced cell death in astrocytes. As shown in Figure 6A, pretreatment of glutamate (100 μM for 24 h) significantly protected the H_2O_2-induced cell. Glutamate alone had no effect on cell viability (Fig. 6A, gray column). Interestingly, such protection by glutamate disappeared when the $P2Y_1$ receptor antagonist MRS2179 was added to the cells 15 min before and during glutamate application (Fig. 6B). We further investigated whether exogenously applied glutamate induces the release of ATP from astrocytes and found that it evoked ATP release that lasted for 15 min (Fig. 6C).

Expression and Function of $P2Y_1$ Receptors in Astrocytes

To elucidate whether $P2Y_1$ receptors are actually expressed and functional in astrocytes, we analyzed the expression of $P2Y_1$ receptors by RT-PCR and mea-